# Analysing jet breakup

## An experimental study on Rayleigh-Plateau instability and subsequent droplet formation

by

C. R. Leliveld

to obtain the degree of Bachelor of Science
at the Delft University of Technology,
to be defended publicly on Tuesday July 24, 2018 at 10:30 AM.


| | | |
|---|---|---|
| Student number: | Leiden: s1212184 | Delft: 4239792 |
| Project duration: | April 23, 2018 – July 24, 2018 | |
| Thesis committee: | dr. ir. H. B. Eral, | TU Delft, supervisor |
| | prof. dr. ir. J. R. van Ommen, | TU Delft, 2nd examiner |




TU Delft

# Preface

You are about to read my bachelor's thesis on jet breakup. As is with probably every bachelor's thesis, it is the first major report I've written, and it couldn't have been done without the help and dedication of others.

Firstly, I'd like to thank my supervisor, Burak Eral, for his time, input, feedback and patience. Thank you for giving me this opportunity to finish my bachelor's study.

Secondly, I'd like to thank Gelmer Bouwman of Kreber B.V. for dedicating much of his time to act as a second supervisor, you have been a tremendous help.

Thirdly, I'd like to thank Prof. Ruud van Ommen for taking the time and interest to serve as a second examiner in the thesis committee.

And last, but definitely not least, I'd like to thank the employees of Kreber B.V. for their warm welcome when I first walked through the door.

*C. R. Leliveld*
*Delft, July 2018*

# Contents

# List of Figures

# List of Tables

# List of Symbols

| Symbol | Description | Standard SI units |
|---|---|---|
| $a$ | Distance between camera lens and nozzle tip | m |
| $A$ | Area | $m^2$ |
| $Bo$ | The Bond number | Dimensionless |
| $D$ | Diameter | m |
| $\eta$ | Dynamic viscosity | Pa s |
| $g$ | Gravitational constant | $m\,s^{-2}$ |
| $\gamma$ | Surface tension | $N\,m^{-1}$ |
| $l$ | Critical length | m |
| $L_D$ | Breakup length | m |
| $Oh$ | The Ohnesorge number | Dimensionless |
| $P$ | Pressure | Pa |
| $\Delta P$ | Pressure gauge | Pa |
| $Q$ | Flow-rate | $m^3\,s^{-1}$ |
| $R$ | Radius | m |
| $Re$ | The Reynolds number | Dimensionless |
| $\rho$ | Density | $kg\,m^{-3}$ |
| $t_s$ | Shutter speed | s |
| $v$ | Velocity | $m\,s^{-1}$ |
| $We$ | The Weber number | Dimensionless |

# Abstract

This report aimed to investigate jet-breakup through nozzles and its dependencies on viscosity, flow-rate and nozzle diameter. By measuring the transition point from dripping to jetting as a function of nozzle diameter and viscosity, it was found that increasing nozzle diameters require increasing flow-rates to reach jetting mode, while increasing viscosity lowers the critical flow-rate for the transition point. The breakup length was also observed to be influenced by both viscosity, flow-rate and nozzle size: increasing either viscosity or flow-rate resulted in an increase of the breakup length. Matching these results in dimensionless form to predictions in literature proved to be difficult, presumably due to the relatively small nozzle diameters used in this research.

# 1 Introduction

## 1.1. Overview of the prilling process

Prilling is, in essence, an industrial crystallisation technique. A liquid melt enters the prilling reactor at the top via nozzles. At the nozzle exit, jets will form that break up into spherical droplets. Cold air is continuously blown through the reactor in the reverse direction (bottom to top), which cools the droplets, allowing them to crystallise. Figure 1.1 shows a schematic overview of a prilling reactor. The end product, which are the spherical crystalline aggregates formed by this process, are called prills.

Figure 1.1: Schematic overview of a prilling reactor. Liquid melt entering at the top, cold airflow cools the droplets down in a countercurrentflow. Image is a courtesy of Kreber B.V.

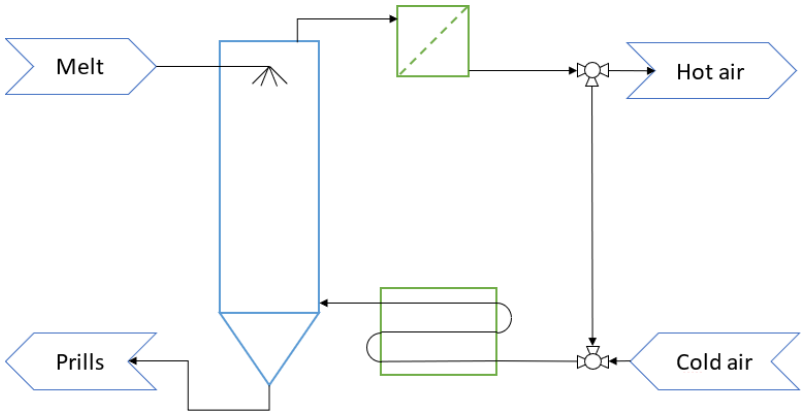


The advantages of prilling over conventional crystallisation techniques, is threefold: firstly, the basic principle behind the reactor is relatively simple, and this makes maintenance and adaptation to product demands easier. This also has relatively low fixed and operational costs as a consequence, when compared to other techniques. Secondly, the prills formed are spherical, which is not only a desirable trait, it also allows the prills to easily roll into the bottom of the reactor for product recovery. Thirdly, contrary to common crystallisation techniques, the prills are not formed while attached to an initiation material (or other crystals), but instead are formed freely in flowing air.

### 1.1.1. Formation of droplets

One of the key processes within the prilling process, is the creation of droplets of a fairly uniform size. As mentioned earlier, the liquid melt enters the reactor through nozzles. At low flow-rates, drops will grow at the nozzle exit and eventually separate from the nozzle and fall down, much like a slightly open water tap that drips. Unfortunately, operating a reactor at low flow-rates results in a relatively slow process, making it uneconomical.

When the flow-rate is increased (and thus our tap turned wide open), a jet will form at the nozzle exit, instead of growing droplets. These jets are inherently unstable [3, 11, 15], and will eventually disintegrate into droplets. Operating at high flow-rates still results in droplet formation, but increases the product formation rate. High flow-rates (jets that break up) are thus preferred over low flow-rates (drips) in industry. Section 2.1.2 deals with the theory behind these processes.

### 1.1.2. Significance

Prilling reactors are not the only application of jet-breakup: many industries make use of droplet formation from jets, for instance, in inkjet printing, spray painting, fuel injection and watering installations in the agricultural industry [11].

Prilling reactors do not operate with a single nozzle. Instead, many nozzles are propelling jets simultaneously to increase the total flow-rate of the reactor. It is important to understand the breakup of these jets, so the resulting droplet size (and thus the size of the end-product: the prill) can be predicted. If the behaviour of the jets can be predicted, and all variables influencing this behaviour are known, then reactors can (more) easily be tailor-made to suit the needs of clients.

### 1.1.3. Research challenges

To create a better understanding of the prilling process, the breakup of jets needs to be studied in-depth. While many articles have been written in the course of time on the subject of jet-breakup, many articles have focussed on very specific parts of jets, or have only posed theories without experimental confirmation. Two very important articles were published that have done both:

The first one: *An experimental study of dynamics of drop formation*, by Xiaguang Zhang and Osman A. Basaran (Phys. Fluids **7** (6), June 1995) offers both theory and experimental results of fluid behaviour, for low flow-rate dripping mode. This article also deals very extensively with drop size distributions and the formation of so-called satellite droplets (see section 2.1.4). While the behaviour of the dripping mode is not the topic of this report, the underlying physics of drips and jets are comparable to an extent. Results of this article and it's theory can therefore be used.

The second article: *Physics of liquid jets*, by J. Eggers and E. Villermaux (Report on Progress in Physics **71**, 2008) is considered the bible on jets. It has effectively combined all available knowledge on jets (up to 2008) and has reported experimental results on several topics. The fact that this article combines the knowledge of so many previously written articles, makes it a very important source for the claims in this report.

Two main areas of interest can be identified for the subject of prilling reactors:

1. Characterization of jet breakup; A jet can breakup differently depending on a plethora of variables. The diameter and shape of the nozzle, the flow-rate, viscosity of the fluid, etc. can all influence the jet breakup. How these parameters influence jet breakup, and especially the size distribution of the droplets, is of interest for the prilling process. To satisfy the needs of customers, it is therefore convenient to be able to accurately predict the shape and size distribution of droplets for given circumstances. For jets, an extensive experimental study has not been done, that has tabulated all experimental data.

2. Propagation of vibrations through the liquid melt; As mentioned before, jets are inherently unstable. This instability (Rayleigh instability) is enhanced by small perturbations affecting the jet, such as vibrations present in the fluid or the surrounding medium. By applying a vibration to the fluid, the jet breakup might be controlled to serve our wishes. Thus, it is of great importance how these waves propagate through the fluid, as they need to reach the nozzle with a high enough amplitude, and the right frequency. Dampening of the fluid (for non-newtonian fluids) and by obstacles in the path of the wave (e.g. a heating element or a filter) might alter these wave characteristics. Being able to predict how a wave will propagate through a given fluid and process configuration, will thus help us optimize the jet breakup.

## 1.2. Focus of report

This report will focus on the former research challenge stated above: the characteristics of jet breakup, and its dependencies on the variables stated above: nozzle diameter and shape, flow-rate and viscosity. The previously mentioned article by Eggers provides much of the theory, while the article by Basaran will mainly provide experimental techniques.

### 1.2.1. Aim of report

This report will mainly consist of an experimental basis for further research. Firstly, the transition from dripping to jetting mode will be investigated. How do physical parameters like viscosity, nozzle diameter

and flow-rate affect this transition point?

Secondly, once the onset of the jetting mode has been pinpointed for multiple situations, how is breakup itself affected by changing the previously mentioned variables? We will investigate the effects of these variables on the jet-breakup, by measuring the length of the jet before breakup occurs, its thickness after a certain distance, and the characteristics of the breakup itself (presence of satellite droplets, form of the neck, etc.).

When possible, results and situations will be expressed in dimensionless form, by using dimensionless numbers that are appropriate for the situation. As this report is a basis for further research, the dimensionless approach is convenient for up- or downscaling of the results in future work.

# 2

# Theoretical Background

## 2.1. Fluid shapes: surface tension, jets and droplets

Since the breakup of jets into droplets is a complex matter, the theoretical background will be broken up into smaller parts. The introduction gave a broad and simple overview of the theory and some of the fundamentals. In this chapter, the theory will be explained to fully understand the experiments, and the parameters that are going to be influenced and measured and what their dependencies are.

### 2.1.1. Fluid deformation

Fluids can take different shapes depending on their situation, but the one characteristic that makes them fluids, is that they flow: they have no fixed shape of itself, and this shape will transform continuously due to forces acting upon the fluid [14]. The forces acting upon a fluid body determine what shape the body will take. For example, fluids at rest settle at the bottom of a container due to gravity, and take on its form.

For this report, we are interested in fluids that are not at rest, but are subjected to changing forces, forcing them to change their shape. Considering a falling body of fluid (of whatever shape), ejected from a nozzle, multiple forces can be identified:

- Forces regardless of circumstances:
  - Gravity acting upon the fluid, pulling it down.
  - Forces due to air-currents interacting with the fluid.
- Forces due to the system:
  - Capillary forces near the tip of the nozzle.
  - Pressure from the syringe pump, driving the fluid through the nozzle.
  - Resistance from tubing and nozzle due to the velocity of the fluid.
- Forces due to shape:
  - Surface tension related forces.
  - Viscous forces, resisting deformation
  - Inertial forces, resisting change of velocity or direction
  - Air resistance due to the velocity of the fluid.

In our case, there are two key parameters that can be controlled easily: the nozzle diameter, and the flow-rate (or pressure) of the syringe pump. The former directly influences the capillary forces, and indirectly affects the velocity of the liquid, given a fixed flow-rate, according to equation (2.1). In this equation, $Q$ equals the flow-rate, $V$ the volume that is pushed through the tube in a given time $t$, and $A$, $D$ and $\bar{v}$ are the area and diameter of the tube and the average velocity of the fluid, respectively.

$$Q \equiv \frac{V}{t} = A \cdot \bar{v} = \frac{\pi D^2}{4} \cdot \bar{v} \qquad \text{or, when isolated for } \bar{v}: \qquad \bar{v} = 4 \cdot \frac{Q}{\pi D^2} \tag{2.1}$$

Due to the fact that the circumference of the jet will change proportional with the diameter of the nozzle, effects of surface tension are also affected (as they are dependent on the circumference of the column).

The controllable flow-rate $Q$ delivered by the syringe pump affects the velocity through the same mechanism stated in equation (2.1).

It is also important to describe some dimensionless quantities that govern the previously mentioned forces:

Table 2.1: List of dimensionless numbers that govern liquid jet systems and droplet formation [20].

| Symbol | Name | Qualitative description | Quantitative description |
|---|---|---|---|
| $Bo$ | Bond | $\frac{\text{gravitational forces}}{\text{surface tension forces}}$ | $\frac{\rho g l^2}{\gamma}$ |
| $Oh$ | Ohnesorge | $\frac{\text{viscous forces}}{\text{surface tension \& inertial forces}}$ | $\frac{\eta}{\sqrt{\rho\gamma l}} = v\sqrt{\frac{\rho}{l \cdot \gamma}} = \frac{\sqrt{We}}{Re}$ |
| $Re$ | Reynolds | $\frac{\text{Inertial forces}}{\text{Viscous forces}}$ | $\frac{\rho v D}{\eta}$ |
| $We$ | Weber | $\frac{\text{inertial forces}}{\text{surface tension forces}}$ | $\frac{\rho l v^2}{\gamma}$ |

The Weber number ($We$) is a measure of the dominance of inertial forces over surface tension forces. A jet with a high Weber number has dominant inertial forces, which is often the effect of a high (squared) velocity. This is also the case in common experience: a jet with a high velocity is harder to deform than a slow-moving drip from a tap. In jets, the Weber number also indicates "…how much a disturbance can grow from one swell to the next." [11].

The Bond number ($Bo$) is somewhat similar to the Weber number in appearance and formula. The difference lies in the fact that the Bond number is a measure of dominance of gravitational forces over surface tension forces. Where $\rho g l^2$ is a measure of potential energy, in contrast to the Weber number's kinetic component, $\rho l v^2$.

While the Reynolds number ($Re$) is not commonly used to describe jets, it is an often used measure of inertial over viscous forces for droplets. In this case, the characteristic length $l$ used in other numbers has been replaced by the droplet diameter $D$, but the numerator remains a measure of kinetic energy.

A combination of viscous, inertial and surface tension forces can be found in the Ohnesorge number ($Oh$). It is a measure of the extent to which viscosity plays a role. As such, it can be expressed as a combination of the Weber and Reynolds numbers.

### 2.1.2. Droplets

When a low flow-rate is passed through a nozzle (a leaky faucet), a droplet accumulates at the tip and grows in time. The capillary forces keep the droplet from falling, until a certain critical volume $V_c$ has been reached [22], at which point the gravitational forces outweigh the capillary forces and the drop disconnects from the nozzle.

This disconnection isn't a clean cut at the nozzle tip. The drop becomes tear-shaped, forms a neck (filament of liquid) between the tip of the nozzle and the primary drop, and this neck stretches until it becomes so thin that it ruptures and the primary droplet falls down [5, 22].

As mentioned before, there are multiple forces at work that determine how exactly such a filament breakup occurs. Multiple studies on the subject have found that there is a distinction between two initial regimes. One where viscous forces dominate and balance the capillary forces ($Oh \gg 1$)[17] and another where inertial forces dominate ($Oh \ll 1$)[6, 9, 13]. Yet, when the thread diameter tends to zero,

it is found that it enters a third regime, in which all three –viscous, inertial and capillary forces– balance each other [5].

While the previously mentioned results on droplet breakup aren't directly applicable to the subject of jets, it does show the importance of the three main forces describing fluid behaviour, and how they are combined in the Ohnesorge number.

### 2.1.3. Jets

The case described above is commonly referred to as the dripping mode. Under certain circumstances, a second mode can be identified: the jetting mode.

When the flow-rate $Q$, and thus the velocity of the fluid emerging from the nozzle, is large enough, a jet of a constant radius will form [3], instead of drops accumulating mass on the tip of the nozzle. The increase in velocity results in larger inertial forces. When these inertial forces become large enough, a jet will form instead of droplets.

The ratio of inertial over surface tension forces is given by the Weber number, and thus the transition point from dripping to jetting mode is often associated with this number. The important role of the fluid velocity is also apparent in its formula, as $We \propto v^2$.

According to Eggers and Villermaux, the transition from dripping to jetting mode occurs when the Weber number is in the order of 1 ($We \geq 1$) [11]. An article by Lin et al. narrows the transition area to $We \approx 8$ [15].

While these are oversimplifications, a more exact approach to understanding when dripping mode turns into jetting mode was taken by Clanet and Lasheras [7]. They pose that the critical Weber number($We_c$) at which transition occurs is a function of the Bond number ($Bo$): the balance of gravitational and surface tension forces determines whether jetting or dripping mode will be present. Clanet and Lasheras came up with a model that describes this transition, which can be seen in equation 2.2.

$$We_c = 4\left[\frac{Bo}{Bo_i}\right]^{1/2}\left[1+\frac{K}{2}(Bo_i\,Bo)^{1/2}-\left(\left(1+\frac{K}{2}(Bo_i\,Bo)^{1/2}\right)^2-1\right)^{1/2}\right]^2 \quad \text{with} \quad K \approx 0.372 \tag{2.2}$$

In this equation, $Bo$ and $Bo_i$ are the Bond numbers for the outer and inner radius, respectively. This model only tested accurately for non-viscous fluids: an increase in the viscosity of the fluid led to a significant error, since viscosity effects are not contained within the model.

### 2.1.4. General jet breakup

When operating within the jetting mode, the cylindrical form of the jet is not the most stable configuration for a liquid. If only a small perturbation of the jet is realised, which is always the case (for instance, when an airflow presses against the jet), then an indentation will be formed in the liquid[3], which propagates through the column in a sinusoidal way, as shown in figure 2.1. Parts of the column can now be described as part of a circle, and local differences in pressure emerge within the jet due to the surface tension. This pressure difference can be described by the Young-Laplace equation [11]:

$$\Delta P = -\gamma \nabla \cdot \underline{n} = \gamma\left(\frac{1}{R_1}+\frac{1}{R_2}\right) \tag{2.3}$$

Where $\Delta P$, $\gamma$ and $\underline{n}$, equal the pressure difference over the liquid-air interface, surface tension of the liquid and the divergence of the normal vector, respectively. For a liquid jet, the normal vector becomes a function of the radius of the jet. Subsequently, in the smaller parts of the jet (the indented parts), the pressure increases with $\frac{1}{R}$, while for the thicker, bulging parts, the pressure decreases because $\frac{1}{R}$ becomes smaller.

Figure 2.1: A cylindrical jet that has become perturbed, starts to show sinusoidal deformations. The smaller part (neck) of the jet experiences an increase in pressure as consequence of the surface tension following the Young-Laplace equation. Analogously, the thicker part experiences a decrease in pressure.[21]

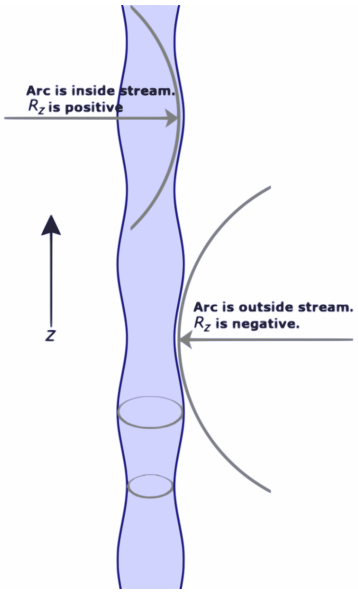

The pressure gradient that exists within the jet, now causes a flux from the smaller parts of the jet towards the thicker parts of the jet. As water is leaving the thinner parts of the jet, the radius becomes even smaller, creating an even greater pressure difference and increasing the flux. This process continues until the indentation in the liquid thread becomes so small, that it ruptures and creates droplets on either end. Apart from the main droplets, very small drops can also formed above the primary droplet, called satellite droplets. These satellite droplets are basically what remains of the small neck of the jet after the rupture has occurred.

The breakup-length $L_D$ signifies the total length of the intact jet until a rupture occurs. This length is dependent on the nozzle geometry and the characteristics of the fluid, prominent among which are the viscosity ($\eta$), velocity, and nozzle radius. Middleman [16] poses a model for this, of which the adapted version by Eral et al. [12] is shown in equation 2.4:

$$\frac{L_D}{2R_o} = 19.5\left(\sqrt{We}(1 + 3\,Oh)\right)^{0.85} \tag{2.4}$$

in which $R_o$ is the outer radius of the nozzle, and $We$, $Oh$ are the Weber and Ohnesorge numbers of the fluid, respectively.

## 2.2. Multiple jet breakup regimes

While all jets are inherently instable [3, 11, 15], the manner in which that instability leads to breakup differs, depending on the circumstances. Reitz and Braco combined the work of four earlier studies to identify four breakup regimes: Rayleigh breakup, first and second wind-induced regime and atomization regime [18], as can be seen in figure 2.2.

Figure 2.2: (a) Rayleigh scattering. (b) First wind-induced regime. (c) Second wind-induced regime. (d) Atomization regime [15]

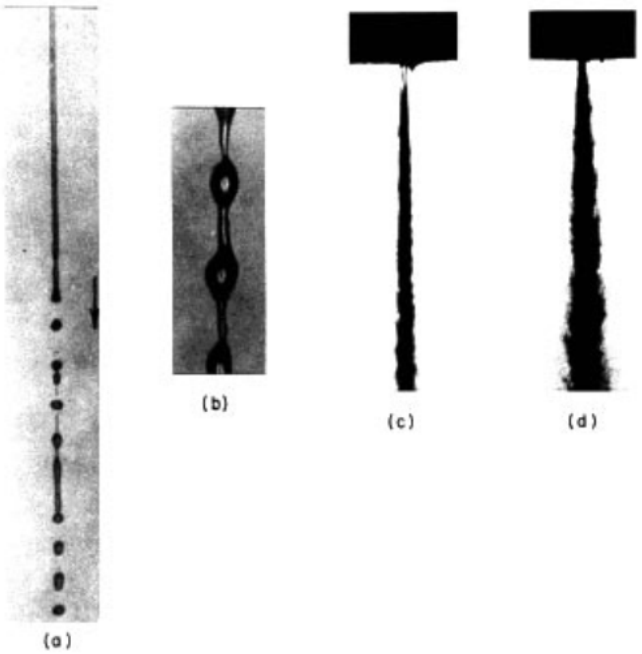


For Rayleigh scattering and the first wind-induced regime, long-wavelength disturbances cause the breakup, due to either imperfections (Rayleigh) and/or interactions with the gaseous medium in which the jet exists (first wind-induced regime). This results in a relatively long process, effecting breakup many nozzle diameters below the nozzle exit [15].

The second wind-induced regime and atomization regime differ from these first two in that the interactions with the gaseous medium causes short-wavelength disturbances which dominate. Droplets become much smaller than the nozzle diameter, and breakup occurs almost instantaneous after leaving the nozzle, producing a spray instead of an actual jet [15].

The Weber number describes the transition from dripping to jetting mode, and also does so for the transition points into other jetting regimes. Lin summarized previous studies and obtained the following criteria for which a certain regime is active [15]:

- For Rayleigh breakup:
  $We_G < 0.4$ or $We_G < 1.2 + 3.41\, Oh^{0.9}$
- For the first wind-induced regime:
  $1.2 + 3.41\, Oh^{0.9} < We_G < 13$
- For the second wind-induced regime:
  $13 < We_G < 40.3$
- For the atomization regime:
  $We_G \geq 40.3$

It is important to note that the Weber number of the liquid ($We_L$) can be used as a measure for the transition from dripping to jetting mode, while it is the Weber number of the surrounding (in our case gaseous) medium ($We_G$) that determines the jet breakup regime. Internal velocity profiles also have a pronounced effect on the jet and its breakup, but this is not considered in the formulation of these criteria [11, 15].

## 2.3. Viscous effects

As mentioned in section 2.1.2, the Ohnesorge number shows the relative strength of viscous forces compared to inertial and surface tension forces. It is therefore an ideal dimensionless quantity to use for jets, as all three forces are affecting jet-breakup and formation.

The viscosity of a liquid measures its resistance to flow [4], or more precisely, its resistance to deformation. Since the flow of liquid is central to this topic, viscosity is going to play a major part. Since general jet breakup is caused by local differences in pressure (the neck and bulging parts of the liquid jet experience different laplace-pressures) as described in section 2.1.4, the resulting flow from this pressure difference will behave differently for a relatively viscous fluid than for a non-viscous fluid.

The previously mentioned section already shows that viscosity is somehow involved in determining the length of a jet before breakup occurs, as can be derived from the presence of the Ohnesorge number in equation (2.4). It also plays a part in determining whether Rayleigh-instability or the first wind-induced regime is active for jets.

# 3

# Method

## 3.1. Experimental set-up

Since multiple experiments were carried out, the equipment used and experimental set-up can differ slightly depending on the experiment. Nevertheless, most experiments can be described using the set-up shown in the schematic of figure 3.1. The exact differences (if present) between this schematic and the set-up used in the experiments will be outlined in its respective sections.

Figure 3.1: Schematic overview of the set-up for most experiments. The syringepump is connected to a vessel using rigid polyethylene tubing. The vessel itself connects the inlet with the outlet (nozzle) and connects two pressure sensors to the system. One pressure sensor with a broad range (0-10 bar), and another with a smaller operating range of 0-700 mbarg. A background was attached behind the nozzle, with a camera and LED light source in front.

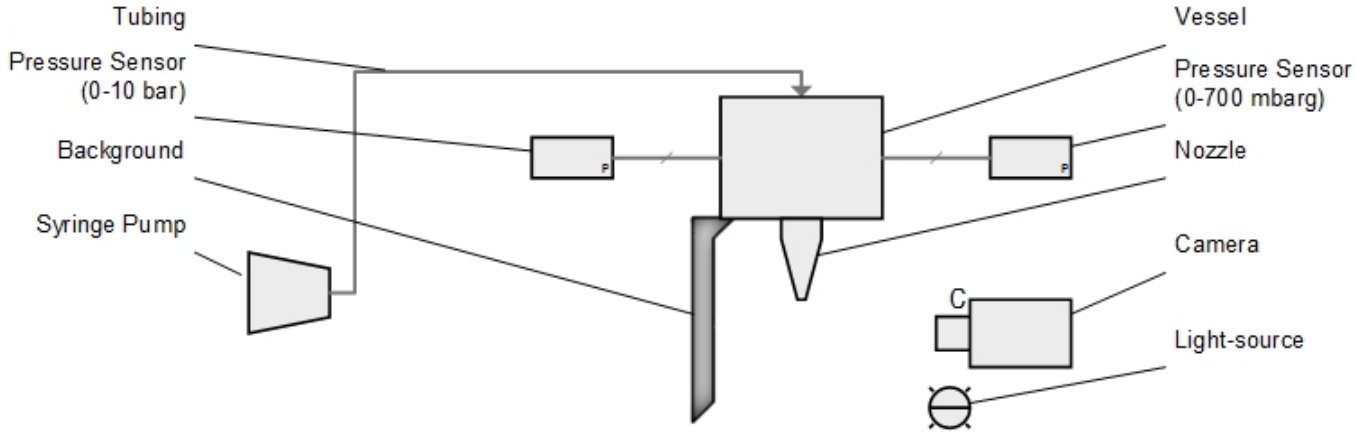


### 3.1.1. Equipment used

A controllable flow-rate $Q$ was provided by a syringe pump (Harvard Apparatus, PHD2000 Infusion) with an accuracy and reproducibility of $\pm 1\%$ and $\pm 0.1\%$, respectively. Operating values for the pump were between 0.0001 µL h$^{-1}$ and 13.249 L h$^{-1}$. Syringes could be used with a volume between 0.5 µL and 140 ml [1].

The syringes used inside the syringe pump were a Terumo® hypodermic 10cc syringe and a Becton Dickinson 60cc syringe. The former has a maximum volume of 12 ml with a measured inner diameter of 15.80 mm. This type of syringe was pre-programmed in the syringe pump, which also showed an inner diameter of 15.80 mm. The latter has a maximum volume of 60 ml, with a measured inner diameter of 26.80 mm, and volumetric accuracy of $\pm 5\%$ [10]. This syringe was also pre-programmed in the syringe pump.

The tips used as nozzle (and as means of injection from syringe to tubing in experiment 1a) are the Nordson Corporation Optimum® General Purpose Tips. These are burr-free, stainless steel tips,

available in a variety of lengths and diameters [8]. The dimensions of the tips used for this experiment can be found in table 3.1. The accuracy of the given nozzle diameters and lengths was not stated by the company.

Table 3.1: Experiment 1a: dimensions of the Nordson Optimum® General Purpose Tips used, in mm, inches and standard wire gauge. [8].

| Colour | Length [mm/"] | Inner diameter [mm/"] | Outer diameter [mm/"] | Gauge (SWG) |
|---|---|---|---|---|
| Lavender | 6.35/0.25 | 0.15/0.006 | 0.31/0.012 | 30 |
| Clear | 6.35/0.25 | 0.20/0.008 | 0.42/0.016 | 27 |
| Red | 6.35/0.25 | 0.25/0.010 | 0.52/0.020 | 25 |
| Blue | 6.35/0.25 | 0.41/0.016 | 0.72/0.028 | 22 |
| Green | 6.35/0.25 | 0.84/0.033 | 1.27/0.050 | 18 |
| Amber | 25.4/1.00 | 1.36/0.053 | 1.65/0.065 | 15 |

A Canon EOS 550D, together with a Canon 100 mm macrolens was used to capture the jet breakup. The camera settings will be displayed in a table for each experiment. A bright LED light source was placed as close to the jet as possible, without being inside the scope of the image. The relatively high brightness of the LED spot was neccesary so the ISO-value and aperture could be set as small as possible.

## 3.2. Locating the transition from dripping to jetting mode by controlling flow-rate for multiple nozzle diameters

As discussed earlier, the transition from dripping to jetting mode is dependent on the Weber number ($We$) of the system. By changing the flow-rate $Q$, the Weber number is changed, proportional to the velocity squared: $We \propto \left(4 \cdot \frac{Q}{\pi D^2}\right)^2$ (mathematics in subsection 2.1.1, equation 2.1).

By slowly increasing $Q$, and thus $We$, the moment at which the transition occurs can be pinpointed, which should lie in the order of 1 and in the neighbourhood of 8. By doing this for different nozzle diameters, the influence of both flow-rate and nozzle diameter on the moment of transition can be measured and the Weber numbers for these different scenario's can be compared.

For each combination of nozzles and a certain $Q$, three photos were taken. The flow-rate was increased in (varying) steps, until jetting mode was reached, after which the flow-rate was then decreased in smaller steps until dripping mode was, again, reached. By repeating this process, the flow-rate at the transition point was measured up to two decimal points.

Determining the transition point was done twice (experiments 1a and b), as the initial set-up of 1a later proved to be inconsistent and had no pressure sensors to check whether the flow-rate was indeed constant. Therefore, the method of both experiments differ.

For both experiments, the results will be compared to the predictions of the model described in equation 2.2.

### 3.2.1. Experiment 1a: flexible tubing, no sensors

For the first experiment, the simplest set-up possible was used, as shown in figure 3.2. It differs from the main set-up by its lack of pressure sensors, a vessel and used other tubing:

Common, (highly-)flexible PVC tubing was used to connect the syringe pump with the nozzle exit. The tubing had an inner diameter of approximately 1.65 mm. Because the tubing was flexible, it could expand when pressure was applied by the syringe pump, which caused some lag and fluctuation in the flow-rate. Unfortunately, the extent of these effects was not measured, due to the absence of a pressure sensor. The length of the entire system was approximately 1.1 m

Table 3.2: Camera settings for experiment 1a, with $a$, $t_s$ and F, being the distance between the end of the lens and the jet, the shutter speed and aperture, respectively.

| $a$ [cm] | $t_s$ [s] | ISO-value | F |
|---|---|---|---|
| $\sim 25$ | $\frac{1}{4000}$ | 800 | 4.0 |

Figure 3.2: Schematic overview of the set-up used. The syringe pump was connected directly to the nozzle via highly flexible pvc tubing. A bright LED spot was used as light source, next to the camera. The background was a black piece of A4 paper with a white circle in the middle (background 1).

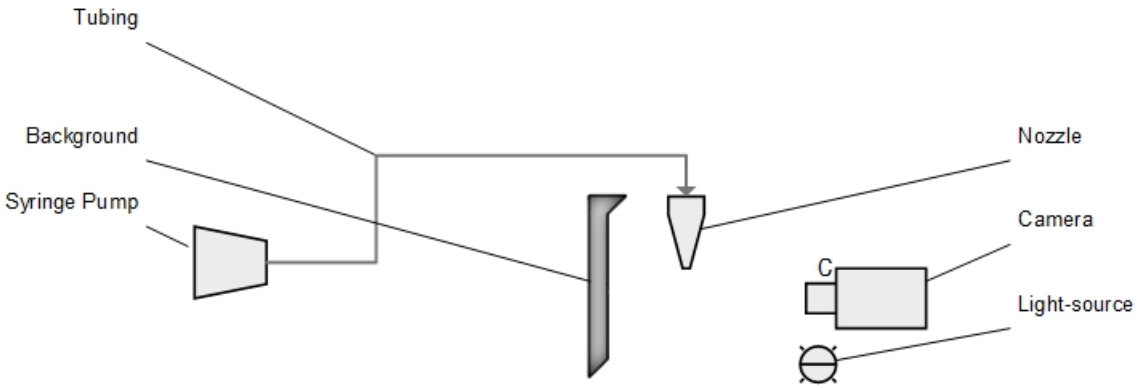


Multiple Terumo® 10cc syringes were used in the syringe pump, as repeated use showed a slight wear of the plunger, creating a stuttering effect on the flow-rate.

Table 3.2 shows the camera settings used for this experiment. The fastest shutter speed possible was chosen to optimally capture the falling droplets and jets. Aperture was set to 4.0, to minimize lens deformation, and the ISO-value was chosen last and kept as low as possible.

An amber tip has approximately the same outer diameter as the inner diameter of the tubing. It was therefore convenient to insert the needles of two amber tips on either end of the tube (and glue the end of the tube to the plastic part of the needle lock). In this way, a leak-free connection was made, which could easily be screwed upon any syringe with a luer lock on the pump-side of the system. Likewise, at the nozzle-exit, the tubing could easily be attached via a luer lock attachment.

### 3.2.2. Experiment 1b: Rigid tubing, pressure sensors to check flow-rate

The set-up of this experiment is exactly as described above in figure 3.1. The function of this reservoir in this experiment is twofold: firstly, it serves as a means to connect the pressure sensors, syringe pump, and nozzles to each other. Secondly, the volume of fluid within the reservoir serves as a buffer for internal velocity differences that exist pre-nozzle.

The vessel had to be bled of air every once in a while. This was done by connecting a small syringe with an amber nozzle via flexible tube to the amber nozzle on the underside of the vessel. The tubing connecting the vessel to the syringe pump was then removed, so water could be injected into the vessel from the bottom, while the air escaped at the top.

The camera settings can be found in table 3.3.

Table 3.3: Camera settings for experiment 1b, with $a$, $t_s$ and F, being the distance between the end of the lens and the jet, the shutter speed and aperture, respectively.

| $a$ [cm] | $t_s$ [s] | ISO-value | F |
|---|---|---|---|
| $\sim 20$ | $\frac{1}{4000}$ | 800 | 4.0 |

## 3.3. Experiment 2: The influence of viscosity on the transition point and jet-breakup

The effects of viscosity are captured in the Ohnesorge number (and Reynolds number for the droplets). To investigate how jet-breakup is affected by changes in viscosity, mixtures of glycerol and water will be used. The viscosity of various different water-glycerol mixtures is documented well, and it is therefore practical to use a mixture of these two fluids.

Using an 87 wt% glycerol-water mixture by Boomlabs B.V. as base (no purity given), five different mixtures, according to table 3.4, were prepared to give a semi-logarithmic progression of viscosity values. In this way, the effects of changes in viscosity can be analysed for a broad range efficiently. This was done for three nozzles: the blue, green and amber nozzle. Smaller nozzles will not be used, as their corresponding pressure is expected to rise above the maximum value to keep the vessel intact.

As Rayleigh instability is our focus, flow-rates will be chosen well above the transition point, so the

Table 3.4: Different glycerol-water mixtures by weight percentage and their corresponding dynamic viscosities ($\eta$) [19], densities ($\rho$) and surface tensions ($\gamma$) [2], as well as the viscosity, density and surface tension of pure water [20], to serve as a frame of reference. *Value extrapolated from source.

| Mixture | Glycerol content [wt%] | $\eta$ [mPa s] | $\rho$ [kg m$^{-3}$] | $\gamma$ [mN m$^{-1}$] |
|---|---|---|---|---|
| Pure water | 0 | 1.002 | 998.02 | 72.86 |
| Glycerol-Water | 50 | 6.00 | 1126.3 | 68.5 |
| Glycerol-Water | 60 | 10.8 | 1153.8 | 67.7 |
| Glycerol-Water | 80 | 60.1 | 1208.5 | 65.4 |
| Glycerol-Water | 85 | 109 | 1221.8 | 64.3 |
| Glycerol-Water | 87 | 153* | 1227.1 | 64.0 |

flow is without a doubt in jetting mode. For each flow-rate, the behaviour of the jet will be documented for pure water, and the glycerol-water mixtures mentioned above. Pure water will be the frame of reference for this experiment, so the different viscosities of the mixtures can be compared easily.

The results of this experiment will be compared with the predictions of the model given by equation 2.2

Qualitatively, the way in which droplet formation occurs (what does the jet-breakup look like?) will be compared for the highly viscous 87 wt% solution and water. Quantitatively, the transition point will once again be determined.

The camera did need some adjustment after a switch in light source (though an LED spot was still being used) and an increase of distance, as can be seen in table 3.5. A smaller aperture was used so droplets diverging towards or away from the lens were more focussed, and the ISO-value was adjusted to compensate for the relative lack of light created by the narrower aperture.

Table 3.5: Camera settings for experiment 2, with $a$, $t_s$ and F, being the distance between the end of the lens and the jet, the shutter speed and aperture, respectively.

| $a$ [cm] | $t_s$ [s] | ISO-value | F |
|---|---|---|---|
| $\sim 30$ | $\frac{1}{4000}$ | 1600 | 11 |

The set-up itself was not changed in essence, and remained as described in figure 3.1 in section 3.1. One pressure sensor was removed (0-700 mbarg) as the pressure of viscous mixtures would destroy the sensitive sensor. The broader 0-10 bar sensor remained.

## 3.4. Experiment 3: Variation of breakup-length due to changes in flow-rate and viscosity

To measure the effect that changes in viscosity and flow-rate have on the length of the jet before breakup occurs, the set-up had to be adjusted slightly. The set-up was moved upwards, to accommodate for the larger height needed to measure long distances before jet-breakup. The background was fitted with a ruler to easily relay height information (see appendix B for an overview of the backgrounds used). The equipment and camera settings used for this experiment has not changed compared to experiment 2 (see section 2.3 and table 3.5 for further details).

At first, the system will be filled with pure water, and all six nozzles will be investigated. For each nozzle, 5 flow-rates will be chosen (as can be seen in table 3.6), ranging from just above the transition point, to twice the flow-rate (linearly spread). Four photo's will be taken of each flow-rate-nozzle combination, and the average breakup length ($< L_D >$) will be reported. Figure 3.3 shows an example of the breakup length.

Secondly, the largest three nozzles (blue, green, amber) will be used in a similar experiment in which the flow-rate is kept constant, but the viscosity is changed. Again, four photo's will be taken of each flow-rate-viscosity combination, and the average length will be reported. The viscosities used will be the same as in experiment 2, by using 87 wt% glycerol and diluting this to achieve lower viscosities. Table 3.7 lists the combinations for this experiment.

From experiment two, a shift of transition point was observed for viscosity changes. Therefore, the flow-rate at which this experiment will be kept constant, will need to be above the transition point of pure water for each nozzle. In this way, jetting mode will be ensured.

Table 3.6: List of all flow-rate-nozzle combinations to be used in experiment three. The flow-rate, $Q$, is given in millilitres per minute, the inner diameter in millimetres.

| Nozzle | Inner diameter [mm] | $Q$ [ml min$^{-1}$] | | | | |
|---|---|---|---|---|---|---|
| Lavender | 0.15 | 2.30 | 2.88 | 3.45 | 4.03 | 4.6 |
| Clear | 0.20 | 3.00 | 3.75 | 4.50 | 5.25 | 6.00 |
| Red | 0.25 | 3.20 | 4.00 | 4.80 | 5.60 | 6.40 |
| Blue | 0.41 | 7.70 | 9.63 | 11.6 | 13.5 | 15.4 |
| Green | 0.84 | 22.0 | 27.5 | 33.0 | 38.5 | 44.0 |
| Amber | 1.36 | 37.0 | 46.3 | 55.5 | 64.8 | 74.0 |

Table 3.7: List of all nozzle-viscosity combinations for experiment three. The dynamic viscosity, $\eta$, is given in millipascal second, the flow-rate, $Q$, in millilitres per minute and the inner diameter in millimetres.

| Nozzle | Inner diameter [mm] | $Q$ [ml min$^{-1}$] | $\eta$ [mPa s] | | | | |
|---|---|---|---|---|---|---|---|
| Blue | 0.41 | 8.00 | | | | | |
| Green | 0.84 | 22.0 | 6.00 | 10.8 | 60.1 | 109 | 153 |
| Amber | 1.36 | 37.0 | | | | | |

Figure 3.3: Example of the breakup length $L_D$ for a jet.

# 4

# Results and Discussion

## 4.1. Experiment 1a: flexible tubing, no sensors

### 4.1.1. Results

In accordance with the method described in section 3.2.1, the following results were obtained:

Table 4.1: Results of experiment 1a, with flexible tubing and no sensors. For each nozzle used, the flow-rate ($Q$) and velocity ($\bar{v}$) corresponding to the transition point has been noted in ml min$^{-1}$ and m s$^{-1}$ respectively, as well as $We_c$ for the liquid at the transition point.

| Nozzle | Inner Diameter [mm] | Outer diameter [mm] | $Q$ [ml min$^{-1}$] | $\bar{v}$[m s$^{-1}$] | $We_c$ |
|---|---|---|---|---|---|
| Lavender | 0.15 | 0.31 | 1.46 | 1.38 | 8.16 |
| Clear | 0.20 | 0.42 | 2.10 | 1.11 | 7.24 |
| Red | 0.25 | 0.52 | 2.95 | 1.00 | 7.25 |
| Blue | 0.41 | 0.72 | 5.45 | 0.688 | 4.73 |
| Green | 0.84 | 1.27 | 13.5 | 0.406 | 2.91 |
| Amber | 1.36 | 1.65 | 22.0 | 0.252 | 1.46 |

### 4.1.2. Discussion

The first three nozzles agree well with the theory by Lin and Reitz: the transition occurs at $We \approx 8$ and at an increasingly high flow-rate for increasing nozzle diameters. Yet, the largest three nozzles see a rapid decrease of $We$ as the diameter grows, only barely remaining above $We = 1$ (the lower limit according to Eggers).

While performing these measurements, it became increasingly hard to differentiate dripping and jetting mode with increasing nozzle diameter. For the smallest three nozzles, the transition could easily be observed with the naked eye. Yet, for the larger three nozzles, the transition 'point' became more of a margin. Flow-rates existed at which jetting and dripping were observed to alternate one another, as can be seen in figure 4.1.

According to Eggers (p. 21) there exists "…a chaotic regime, that lies between periodic dripping and jetting." [11]. Closer examination of pho-

Figure 4.1: Alternation between dripping and jetting mode. The last droplet was formed as a result of dripping mode, making it a relatively large drop ($D_{drop} \gg D_{in}$), while the other droplets are significantly smaller ($D_{drop} \approx D_{in}$). These were formed as a result of jetting mode. The filament is also different from characteristic dripping or jetting mode necks.

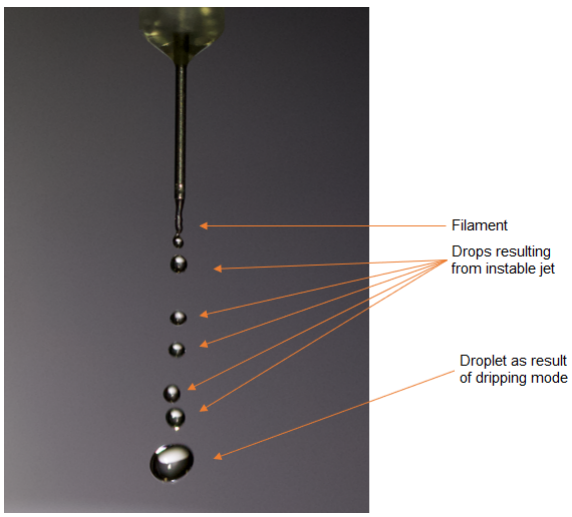

tographs taken in this experiment and Eggers article, reveal that this chaotic regime is indeed present, as can be seen in figure 4.3.

Nevertheless, figure 4.2 shows a close resemblance with the calculated Weber number, following the predictions of equation 2.2.

Figure 4.2: Graph of the critical Weber number ($We_c$) of the transition point versus the corresponding Bond number $Bo$ of the nozzles (calculated using the outer diameter). The orange line shows the predicted $We_c$ (following equation (2.2)), while the blue line shows the measured $We_c$

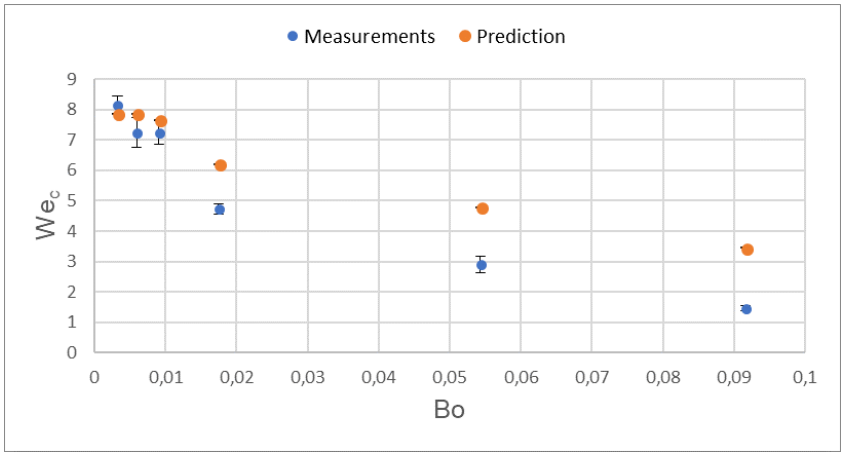


### 4.1.3. Questionable results

The presence of a chaotic regime, which was seemingly absent at smaller diameters, and the resulting difficulty in determining whether dripping or jetting mode was active, is one of the reasons why the results for the blue, green and amber nozzles are highly questionable.

A second reason is the usage of flexible tubing. Larger nozzle diameters require a larger flow-rate to obtain similar Weber numbers. Since the flow-rate is pressure-driven, the pressure within the tubing is increasing proportional to the flow-rate. As such, some of the pressure is effectively used to expand the tubing, instead of driving a flow-rate. This increases the volume of the system, which needs to be filled with liquid, meaning $Q_{in} \neq Q_{out}$. This effect is of a temporary nature: once the tube is expanded to the extent corresponding with the pressure, and the tubing is filled with fluid, $Q_{in}$ will once again be equal to $Q_{out}$. This steady state was never reached for the largest three nozzles however, since the volume of the syringe (10 ml) was inadequately small.

Figure 4.3: The left image, taken from the article by Eggers [11], in which (a) shows dripping mode ($We = 0.031$), (b) shows chaotic dripping ($We = 0.86$), and (c) shows jetting ($We = 1.15$). Diameter (inner or outer not specified) of the nozzle is 2.16 mm. The right image shows the Amber nozzle (inner diameter of 1.36 mm) at $We = 2.67$

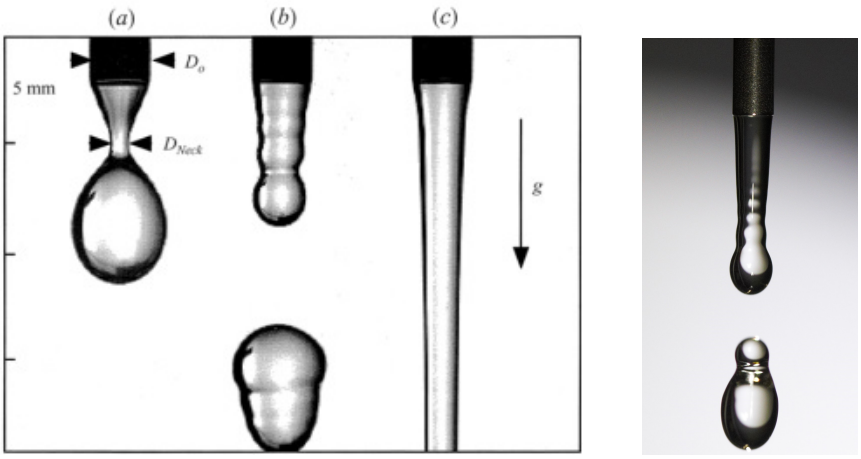

## 4.2. Experiment 1b: rigid tubing and pressure sensors

### 4.2.1. Results

In accordance with the method described in sections 3.2 and 3.2.2, the following results were obtained:

Table 4.2: Results of experiment 1b, with rigid tubing and two pressure sensors. For each nozzle used, the flow-rate ($Q$) and velocity ($\bar{v}$) corresponding to the transition point has been noted in ml min$^{-1}$ and m s$^{-1}$ respectively, as well as $We_c$ for the liquid at the transition point. The pressures at the transition point were also added, where $\bar{P}$ is the average absolute pressure in bar and $\Delta P$ is the relative pressure in mbarg (millibar gauge). * = not measured due to faulty sensor.

| Nozzle | Inner Diameter [mm] | Outer diameter [mm] | $Q$ [ml min$^{-1}$] | $\bar{v}$[m s$^{-1}$] | $We_c$ | $\bar{P}$ [bar] | $\Delta P$ [mbarg] |
|---|---|---|---|---|---|---|---|
| Lavender | 0.15 | 0.31 | 2.00 | 1.89 | 15.1 | 1.35 | -* |
| Clear | 0.20 | 0.42 | 2.85 | 1.51 | 13.2 | 1.158 | 135 |
| Red | 0.25 | 0.52 | 3.05 | 1.04 | 7.66 | 1.089 | 66.0 |
| Blue | 0.41 | 0.72 | 7.50 | 0.947 | 8.86 | 1.048 | 23.5 |
| Green | 0.84 | 1.27 | 21.0 | 0.632 | 6.96 | 1.026 | 2.5 |
| Amber | 1.36 | 1.65 | 36.0 | 0.413 | 3.87 | 1.023 | 0.0 |

### 4.2.2. Discussion

The presence of a chaotic regime, and the distinction between chaotic and jetting mode, drastically changed the moment at which the transition occurs. Table 4.2 shows that the critical Weber numbers at which the transition occurs, are significantly higher for all nozzles, when compared with the results of experiment 1a in table 4.1.

Figure 4.4: Graph of the critical Weber number ($We_c$) of the transition point versus the corresponding Bond number $Bo$ of the nozzles (calculated using the outer diameter). The orange line shows the predicted $We_c$ (following equation (2.2)), while the blue line shows the measured $We_c$

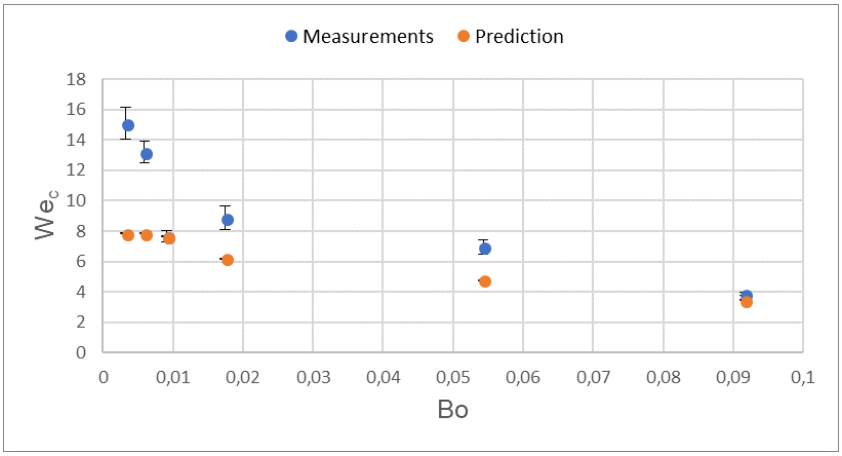


The lavender and clear nozzle show Weber numbers that far exceed both criteria ($We$ order of 1 & $We \approx 8$), while the red, blue and green nozzles agree with these criteria very well. The amber nozzle still falls short of the posed criteria.

While different ways of calculating the Weber number might alter it to some extent (for instance by choosing another critical length), the measured values do not agree with Lin's criteria of $We \approx 8$. In the article by Eggers, nozzle diameters were typically within the range of 1-10 mm. Since the chosen nozzles are significantly smaller, the delicate balance of forces that leads to jet-behaviour might be different for this scale of nozzle, causing the Weber numbers to rise. This would also explain why some of the larger diameter nozzles do agree with Eggers work.

Figure 4.4 shows that the results are not similar to the calculations. Yet, if we accept that the result of the red nozzle was a faulty measurement, the graph starts to bear the resemblance of the calculations,

except for Weber numbers being slightly higher for all data points. Increasing nozzle size shows an increasingly closer match to the model. Thus, an explanation for the mismatch of results and prediction might be that for relatively small nozzle sizes, the model does not hold.

Figure 4.5: Pressure oscillations remaining in vessel with a flow-rate of 3.4 ml $min^{-1}$ through the red nozzle

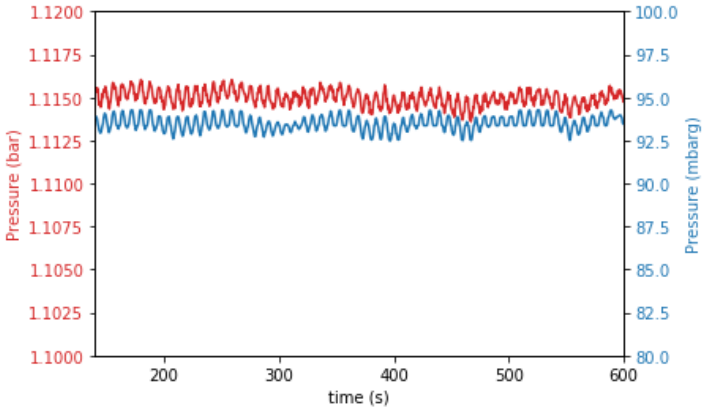


The pressures shown in table 4.2 show that smaller nozzles have a larger resistance to flow than larger nozzles. Jets did not always occur at a given pressure, instead, the results of the amber nozzle show that once a certain threshold has been crossed, the pressure difference between the interior and exterior of the vessel becomes negligible. The resistance to flow for smaller nozzles meant that pressure needed to be built up within the vessel. The initial build-up occurred with an exponential decrease, after which stabilizing at a certain value. However, not all oscillations were eliminated after stabilization. A certain oscillation with a period of approximately 7.5 s remained in nearly all measurements, as can be seen in figure 4.5. This oscillation was probably caused by the pitch of the syringe pump.

## 4.3. Experiment 2: The influence of viscosity on the transition point and jet-breakup

This experiment adds the dimension of viscosity to jet-breakup. Viscosity has a large impact on fluid behaviour, and therefore the experimental set-up. Originally, all nozzles were supposed to be investigated with different viscosities, yet the set-up was not build to withstand great pressures. For the most viscous fluid (87 wt% glycerol), the lavender nozzle was nowhere near reaching steady flow and had already surpassed 4.5 bar when a tube disconnected (the vessel was originally built for $\pm 2$ bar.

To prevent instability of the set-up itself, some of the smaller nozzles have been left out for certain experiments, and, in the case of the lavender nozzle, will not be used at all.

Furthermore, this section will also deal with some of the qualitative aspects of viscous flow that were observed, but which were not necessarily mentioned in the method section (3.3) of this report.

### 4.3.1. Results

The results of experiment two are listed in table 4.3. Originally, the red and green nozzle were supposed to be used for this experiment. However, due to the pressure issues mentioned above, the red nozzle was replaced for the blue nozzle with a slightly larger diameter. The amber nozzle was added halfway purely for photographic purposes, though the data will be used as well.

### 4.3.2. Discussion

By calculating the critical Weber and Ohnesorge numbers for each experiment, dimensionless results are obtained which might be correlated to one another. Since $Oh$ is the characteristic dimensionless number that combines all major forces affecting jet breakup with viscosity, and $We$ is associated with the dripping to jetting transition, a trend might be discovered connecting the influence of viscosity to the transition point.

Table 4.3: Results of experiment two. The observed flow-rates corresponding with the transition point for the specific nozzle-viscosity combinations are listed. From this data, the critical Weber number $We_c$ and the Ohnesorge number were calculated that belonged to the transition point. The last two values for the amber nozzle are missing, since the nozzle was originally not meant to be used, but halfway through the experiment the amber nozzle was added for extra clarity on images (the amber nozzle is easy to photograph clearly due it's larger size).

Throughout the experiment it was observed that an increase of viscosity, resulted in a decrease of the required flow-rate for dripping-jetting transition.

| | | $\eta$ [mPa s] | | | | | |
|---|---|---|---|---|---|---|---|
| Nozzle | | 1.002 | 6.00 | 10.8 | 60.1 | 109 | 153 |
| Blue | $Q$ [ml min$^{-1}$] | 7.50 | 6.30 | 6.25 | 6.0 | 6.0 | 5.50 |
| | $We_c$ | 8.85 | 7.04 | 7.10 | 6.86 | 6.93 | 5.85 |
| | $Oh$ | $4.38 \times 10^{-3}$ | $2.55 \times 10^{-2}$ | $4.55 \times 10^{-2}$ | 0.252 | 0.458 | 0.643 |
| Green | $Q$ [ml min$^{-1}$] | 21.0 | 16.5 | 15.5 | 15.0 | 14.0 | 12.8 |
| | $We_c$ | 6.94 | 4.84 | 4.37 | 4.29 | 3.78 | 3.17 |
| | $Oh$ | $3.30 \times 10^{-3}$ | $1.92 \times 10^{-2}$ | $3.43 \times 10^{-2}$ | 0.190 | 0.345 | 0.484 |
| Amber | $Q$ [ml min$^{-1}$] | 36.0 | 32.0 | 29.0 | 22.0 | - | - |
| | $We_c$ | 3.86 | 3.44 | 2.89 | 1.74 | - | - |
| | $Oh$ | $2.90 \times 10^{-3}$ | $1.68 \times 10^{-2}$ | $3.01 \times 10^{-2}$ | 0.166 | 0.303 | 0.425 |

Figure 4.6 shows a plot of the Ohnesorge values for the viscosity-nozzle combinations versus their corresponding critical Weber number. Unfortunately, no real trend was discovered. Nevertheless, it confirms the fact that $Oh$ does have an influence on the transition point for this range, and that an increase in Ohnesorge means a decrease in the critical Weber number. This was to be expected, as literature indicates the same result of no obvious trend or correlation between Ohnesorge and critical Weber [12].

The effects of viscosity on the transition point are observable, and since it is the only parameter that has been significantly changed, must also be the cause of the shift. Nevertheless, a suitable mathematical explanation of how viscosity influences that point could not be found.

### 4.3.3. Qualitative differences in jet breakup between viscous and non-viscous fluids

Fluids with a relatively high viscosity are different in many ways when compared to pure water. Yet, not all these aspects are quantifiable, and certainly not all differences were supposed to be quantified for this experiment. Nevertheless, some observations were made during this experiment, that are of importance to the next experiment, and to give a better understanding of the exact mechanism of breakup. The nature of the perturbations leading to breakup and satellite droplet formation will be discussed.

Figure 4.7 shows two typical water jets, and three very viscous jets. Firstly, the nature of the perturbations is very different for the viscous and non-viscous jet. For the jets of pure water, when the perturbations have started, fast, and very small wavelength perturbations grow towards breakup (capillary waves). The time scale of this is extremely fast (the camera already has trouble capturing it clearly with a shutter speed of $\frac{1}{4000}$ s), and the length from the first noticeable perturbation until breakup is typically in the order of millimetres.

The relatively viscous jets behave differently: their perturbations start long before breakup, and continue for centimetres before eventually causing breakup. The viscous jets create long thin threads in between bulges instead of the fast rippling effect of the water jets. The time scale is significantly larger, as the same droplet could sometimes be recognized on the next image.

This difference in time scale between viscous and non-viscous fluids is purely caused by the resistance to flow of a viscous fluid. Eventually, the viscous thread ruptures, either at one end, or both ends. The fourth image of figure 4.7 shows a rupture at both ends. A satellite droplet will form with the remains of this thread, which is noticeably smaller in diameter than primary droplets (as can be seen in the third image). If the thread only ruptures at one end, then it can either retract into the primary droplet

Figure 4.6: Scatter plot of the dimensionless results of experiment two. The Ohnesorge number, signifying the effects of viscosity, versus the critical Weber number, signifying the transition point, show no real trend. or correlation.

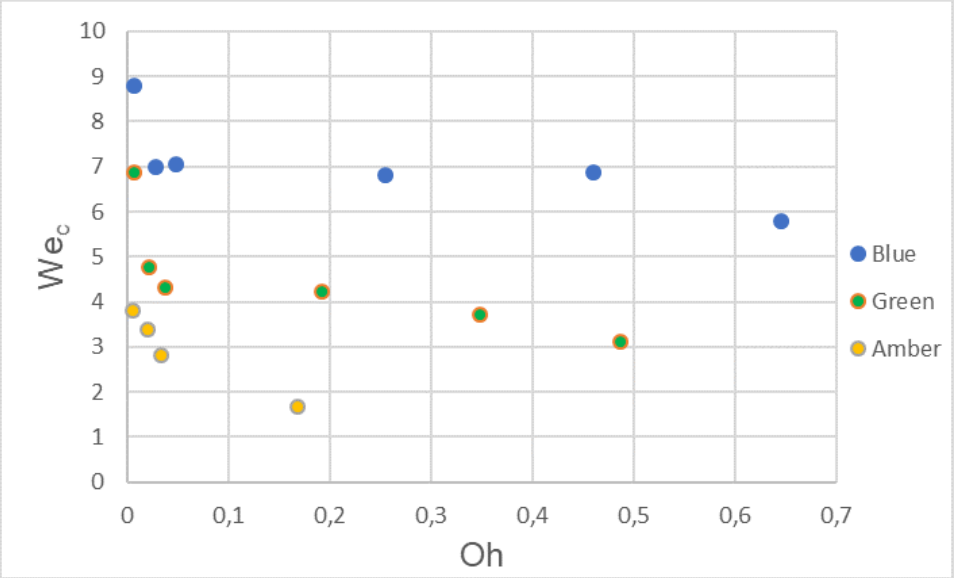


Figure 4.7: Typical jets for pure water (left) and 87wt% glycerol (right). All images are of a green nozzle, except the rightmost image, which was taken of an amber nozzle.

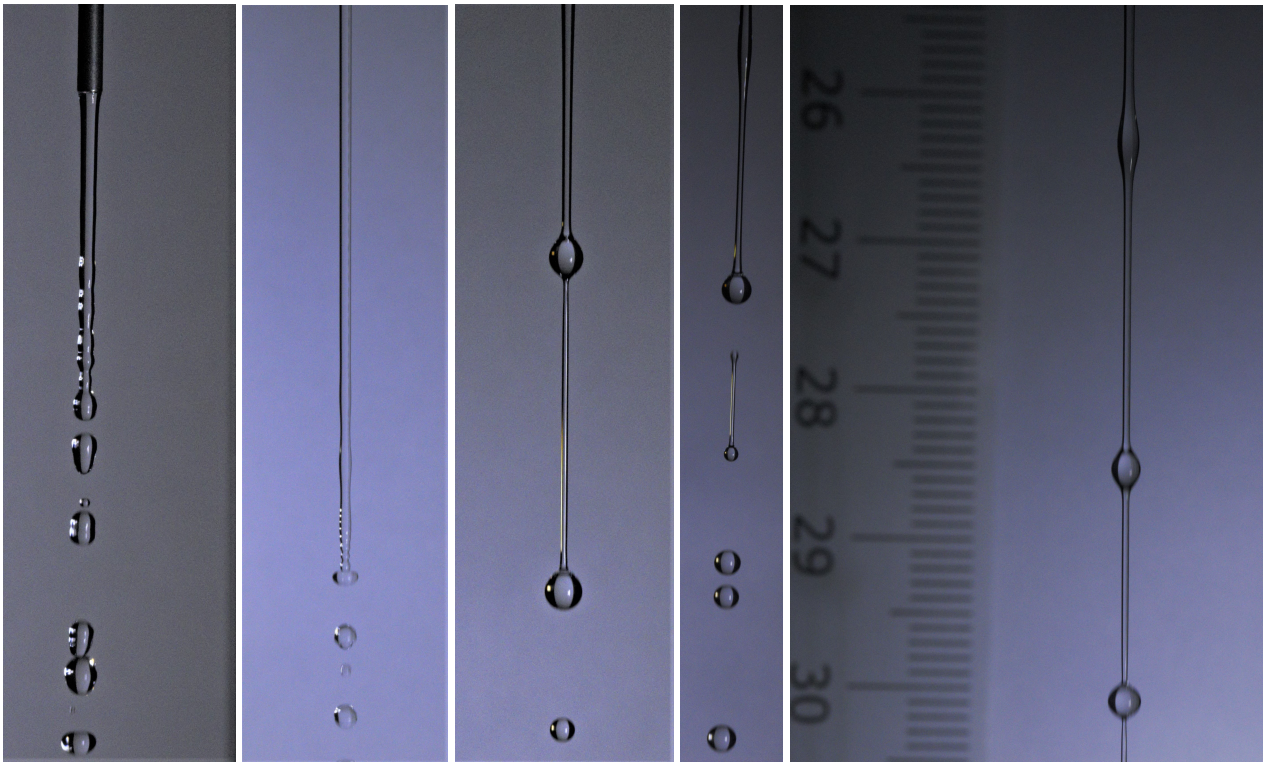

it is still attached to, or create another satellite droplet if it manages to separate at the other end.

This creates multiple possible sizes of satellite droplets, depending on the way it was formed. This effect is not noticeably present on photo's of water jets. In fact: not a single photo of a water jet showed the actual formation of satellite droplets. Only their existence was sporadically captured on photographs, contrary to photographs of viscous fluids: only a small amount of photo's of viscous fluids showed no satellite droplets, nor their formation. Therefore, it seems that satellite droplets are easier to form for a highly viscous fluid, than for non-viscous fluids.

## 4.4. Experiment 3: Variation of breakup-length due to changes in flow-rate and viscosity

As the datasets for the entire experiment are considerably large, tables containing the entirety of the data collected, can be found in appendix A. This section will only state the end-results of the experiments, as well as their interpretation and discussion. Firstly, the part of the experiment with a variable flow-rate will be discussed, followed by the part dealing with viscosity changes.

### 4.4.1. Variable flow-rate: results

An increase in flow-rate, should also increase the breakup-length, $L_D$. Table 4.4 shows that for all nozzles, this was indeed the case.

Table 4.4: Overview of the results of experiment 3 for variable flow-rate, where $Q$, $< L_D >$, $R_{in}$, and $We$ are the flow-rate, average breakup-length, inner radius of the nozzle and the Weber number, respectively. $\frac{< L_D >}{2R_{out}}$ signifies the breakup-length normalized by the outer radius of the nozzle.

| Nozzle | $Q$ [ml min$^{-1}$] | $< L_D >$ [mm] | $\frac{< L_D >}{2R_{out}}$ | $We$ |
|---|---|---|---|---|
| Clear | 3.00 | 3.48 | 8.27 | 14.6 |
| | 3.75 | 11.7 | 27.9 | 22.8 |
| | 4.50 | 14.3 | 34.1 | 32.9 |
| | 5.25 | 17.6 | 41.8 | 44.7 |
| | 6.00 | 20.4 | 48.6 | 58.4 |
| Red | 3.20 | 3.07 | 5.90 | 8.43 |
| | 4.00 | 4.55 | 8.75 | 13.2 |
| | 4.80 | 14.1 | 27.1 | 19.0 |
| | 5.60 | 17.5 | 33.7 | 25.8 |
| | 6.40 | 19.8 | 38.0 | 33.7 |
| Blue | 7.70 | 5.70 | 7.92 | 9.34 |
| | 9.63 | 23.0 | 32.0 | 14.6 |
| | 11.6 | 30.2 | 41.9 | 21.2 |
| | 13.5 | 36.3 | 50.4 | 28.7 |
| | 15.4 | 41.4 | 57.5 | 37.4 |
| Green | 22.0 | 36.6 | 28.8 | 7.63 |
| | 27.5 | 53.2 | 41.9 | 11.9 |
| | 33.0 | 65.2 | 51.4 | 17.2 |
| | 38.5 | 73.8 | 58.1 | 23.4 |
| | 44.0 | 91.3 | 71.9 | 30.5 |
| Amber | 37.0 | 59.1 | 35.8 | 4.08 |
| | 46.3 | 76.0 | 46.0 | 6.39 |
| | 55.5 | 92.7 | 56.2 | 9.19 |
| | 64.8 | 105 | 63.6 | 12.5 |
| | 74.0 | 107 | 64.6 | 16.3 |

### 4.4.2. Variable flow-rate: discussion

To compare these results to literature, $\frac{L_D}{2R_{out}}$ will be calculated for each flow-rate according to the model described by equation 2.4. Since only pure water was used for this part with a corresponding Ohnesorge number of $Oh = 0.003 \ll We$, the equation can be simplified to the following:

$$\frac{L_D}{2R_{out}} = 19.5\left(\sqrt{We}(1 + 3\,Oh)\right)^{0.85} = 19.5\sqrt{We}^{0.85} = 19.5\,We^{0.425} \tag{4.1}$$

Figure 4.10 shows the result of the comparison. It is clear that while the calculated and measured values are not identical, they do take on the same form or trend. The first data points for the clear (a) and blue nozzle (c) , and the first two data points for the red nozzle (b), do not follow the trend clearly. The photo's taken during these experiments show that this was a method error: these data points belong to the chaotic regime instead of jetting mode, as can be seen in figure 4.8.

Figure 4.8: Shows why some of the data points are invalid for figure 4.10. All 'jets' are actually a manifestation of chaotic dripping mode.

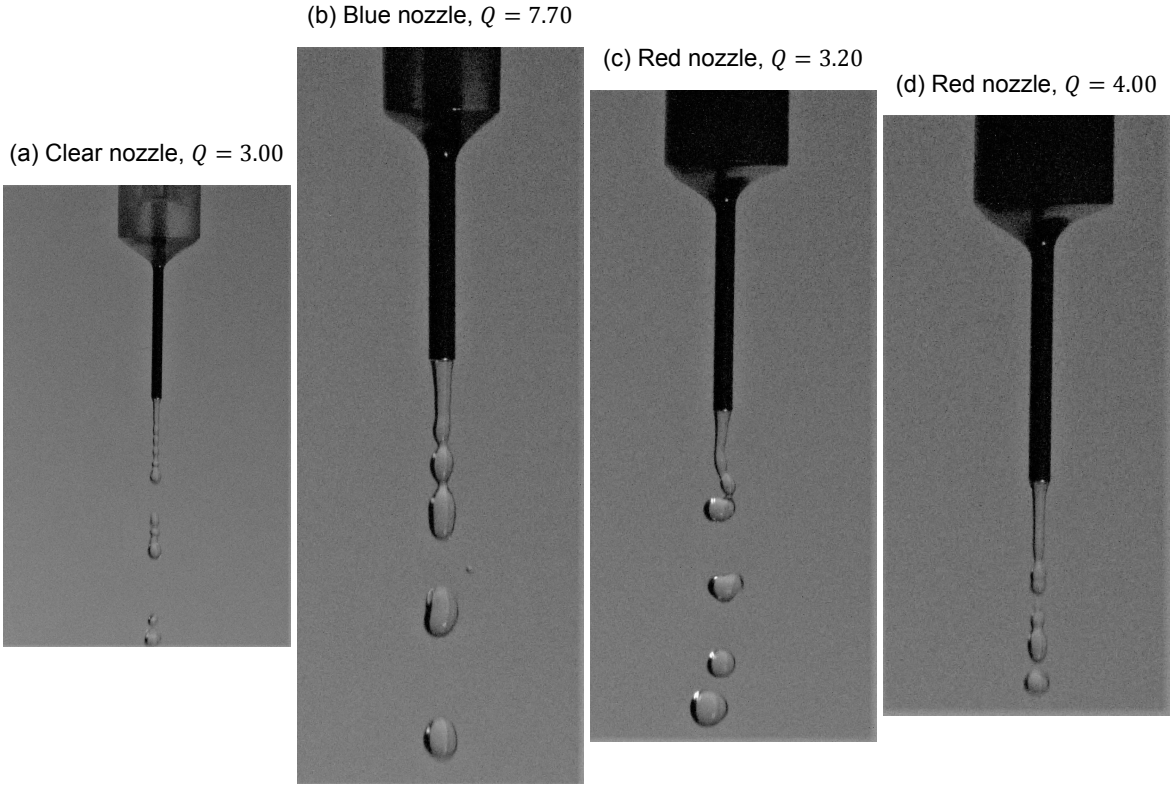


After ignoring the erroneous data points, the measured graphs follow the same trend as the calculated graphs (within a margin of error). Therefore, the underlying relationship between the breakup-length and the Weber number must be valid, meaning $\frac{L_D}{2R_{out}} \propto 19.5\,We^{0.425}$. This dependency on the Weber number shows that the flow-rate $Q$ (and therefore $\bar{v}$) directly influences the breakup-length of a jet.

It is also important to note the margin of error for this experiment. The error in all measurements is twofold: first and foremost, the distance between nozzle and jet breakup was determined by reading a ruler attached to the background. While this ruler was adequately accurate, the lens used to photograph the situation will always distort its image to some degree. A point photographed above the lens will always read with a negative error, while a point below it will always be read with a positive error, as illustrated by figure 4.9.

Secondly, the exact breakup length changes continuously within a margin. For example, just before the rupture occurs, a large breakup length will be recorded. Similarly, just after the rupture a shorter one will be recorded, as the filament connecting the previous droplet has either formed a satellite droplet, or retracted into the new primary droplet, which is located closer to the nozzle.

This difference is the reason why 4 to 6 images of the same situation were combined to form an average length. While this reduces the differences in breakup-length, an error margin still exists.

Figure 4.9: Shows the (overstated) effect of camera distortion on the measurement error. An object above the lens will always be recorded with a negative error to position. Inversely, an object below the lens will be recorded with a positive error.

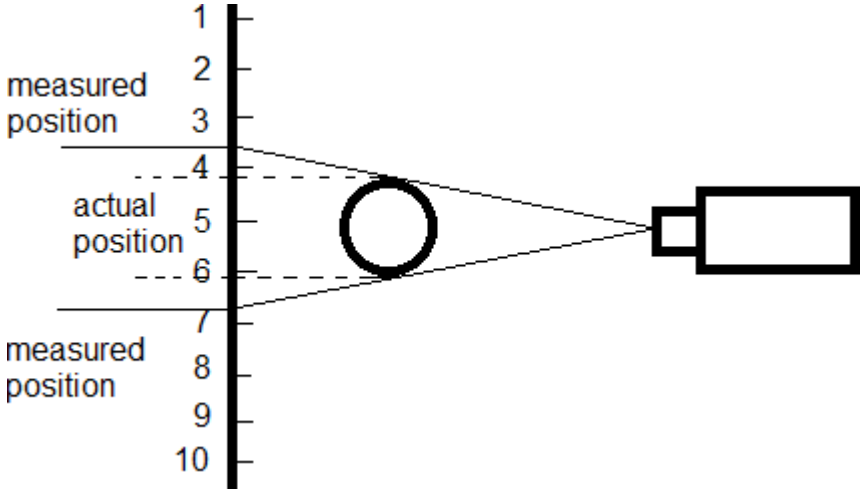

Figure 4.10: Plots of the measured breakup-length $L_D$, normalized by the outer radius $R_{out}$ versus the Weber number $We$. The orange line signifies the calculated $L_D$, while the line corresponding with the nozzle colour shows the measured values. While the calculated value of $L_D$ is too large for (a) to (d), the trend which they follow shows similarities.

(a) Clear nozzle

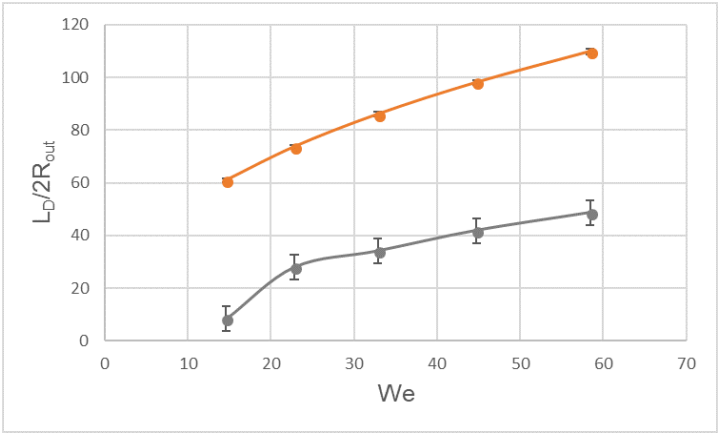


(b) Red nozzle

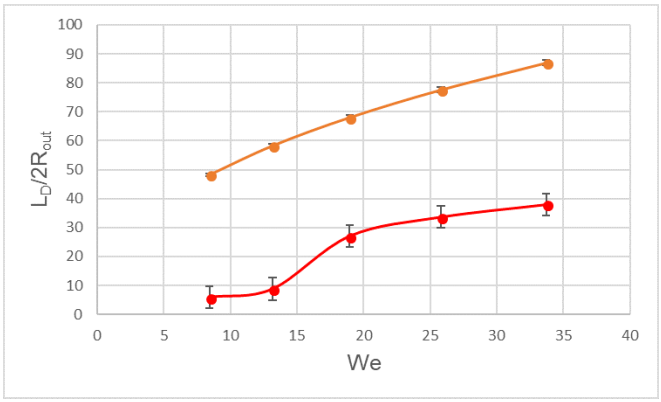


(c) Blue nozzle

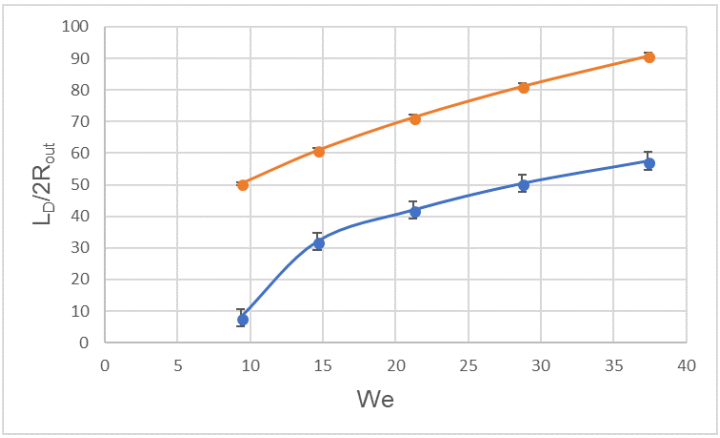


(d) Green nozzle

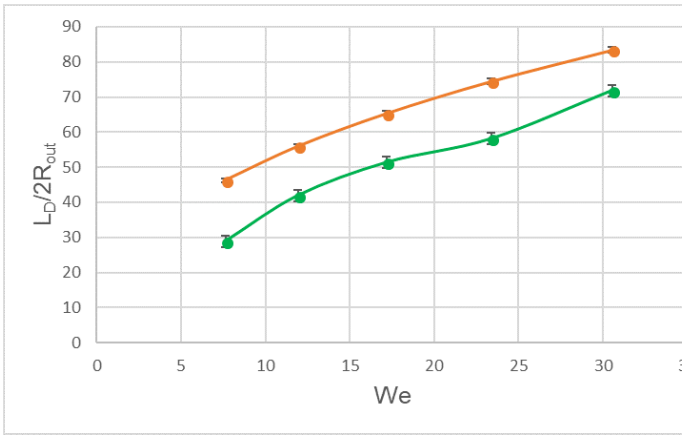


(e) Amber nozzle

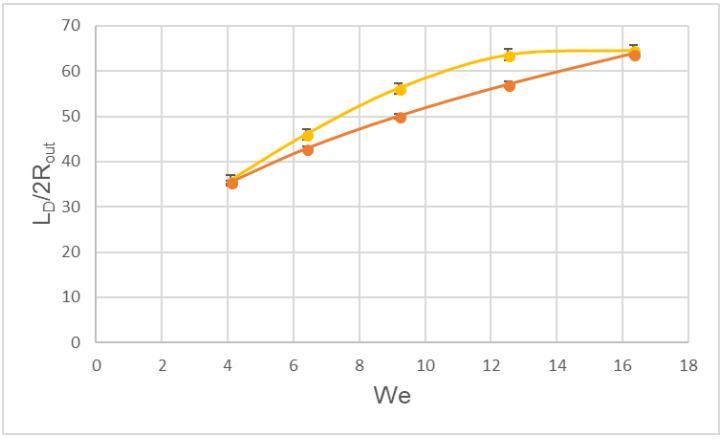


### 4.4.3. Variable viscosity: results

Due to an error in the lab work, a solution of 70 wt% glycerol was used next to the described glycerol-water mixtures. While not originally planned, the extra data point provides extra information, and has been added to the results. Table 4.5 shows the average length before jet breakup, corresponding to the nozzle-viscosity combination.

Table 4.5: Results of experiment three, where the breakup length $L_D$ was measured for multiple glycerol solutions of different viscosities $\eta$ and for different nozzles at a fixed flow-rate. The table also lists the normalized breakup length $\frac{L_D}{2R_{out}}$, with $R_{out}$ being the outer radius of the nozzle. The Ohnesorge number has been listed for all situations.

| | | Fluid mixtures and their viscosity | | | | | | |
|---|---|---|---|---|---|---|---|---|
| | Glycerol fraction [wt%] | 0 | 50 | 60 | 70 | 80 | 85 | 87 |
| | $\eta$ [mPa s] | 1.002 | 6.00 | 10.8 | 22.5 | 60.1 | 109 | 153 |
| Blue nozzle, $Q = 8.00\,\mathrm{ml\,min^{-1}}$ | $< L_D >$ [mm] | - | 13.9 | 14.1 | 17.3 | 21.7 | 29.5 | 36.5 |
| | $\frac{<L_D>}{2R_{out}}$ | - | 19.3 | 19.5 | 24.1 | 30.1 | 40.9 | 50.6 |
| | $Oh$ | - | 0.0254 | 0.0455 | 0.0944 | 0.252 | 0.458 | 0.643 |
| Green nozzle, $Q = 22.00\,\mathrm{ml\,min^{-1}}$ | $< L_D >$ [mm] | 36.4 | 30.5 | 27.0 | 37.4 | 48.6 | 72.5 | 89.2 |
| | $\frac{<L_D>}{2R_{out}}$ | 28.7 | 24.0 | 21.3 | 29.4 | 38.3 | 57.1 | 70.2 |
| | $Oh$ | 0.00330 | 0.0192 | 0.0343 | 0.0710 | 0.190 | 0.345 | 0.484 |
| Amber nozzle, $Q = 37.0\,\mathrm{ml\,min^{-1}}$ | $< L_D >$ [mm] | 59.4 | 50.8 | 55.2 | 53.6 | 71.1 | 108 | 136 |
| | $\frac{<L_D>}{2R_{out}}$ | 36.0 | 30.8 | 33.5 | 32.5 | 43.1 | 65.6 | 82.5 |
| | $Oh$ | 0.00289 | 0.0168 | 0.0301 | 0.0624 | 0.166 | 0.303 | 0.425 |

### 4.4.4. Variable viscosity: discussion

While this part of the experiment was very similar to the earlier part, it proved to be more difficult to determine the breakup-length. The very viscous solutions have a relatively large time scale for the actual breakup process, as discussed in section 4.3.3. This causes the necks before breakup to extend for a relatively large length, before finally rupturing. The margin of error (which was discussed for the previous part of this experiment) caused by small differences in breakup length is enhanced greatly by the viscous effects of these solutions.

In the previous part, the minima and maxima for each situation lay apart by approximately 2-5 mm. For this part, that spread was much larger, in some cases reaching differences up to 2.6 cm, as shown in figure 4.11. Averaging the results of 6 images proved to be an adequate measure for the previous part, yet for large differences like those observed for this part, the error margin becomes significantly larger.

Similar to the previous part, the normalized breakup length has been plotted against the Ohnesorge number, with the addition of the predictions of equation (2.4), shown in figure 4.12.

The predictions do not match the observed values, even with the large error margin that was previously discussed in mind. The predictions even seem to indicate the opposite of what was observed: the observed data shows that a decrease in nozzle size leads to a flatter slope (smaller nozzles seem to be affected by viscosity less intense than larger nozzles), while the prediction shows a steeper slope for decreasing nozzle size.

The mismatch between the prediction and results may be caused by the fact that the nozzles are relatively small. As with other experiments carried out in this report, the graph shows that the amber nozzle starts to line up with the prediction (in fact, the begin and end-point are nearly the same). The same was seen in figure 4.10 (e) (the $\frac{L_D}{R_{out}}$ vs $Q$ experiment) and figure 4.4 ($We_c$ vs $Bo$ experiment), where the amber nozzle starts to show similarities, while the smaller nozzles are increasingly mismatched.

Figure 4.11: Comparison of two images, showing the large difference in breakup length for the same situation: 80wt% of glycerol through an amber nozzle, at $Q = 37.0\,\mathrm{ml\,min^{-1}}$. the left image shows the position of breakup at 22.19 cm, while the right image shows that position at 24.78 cm.

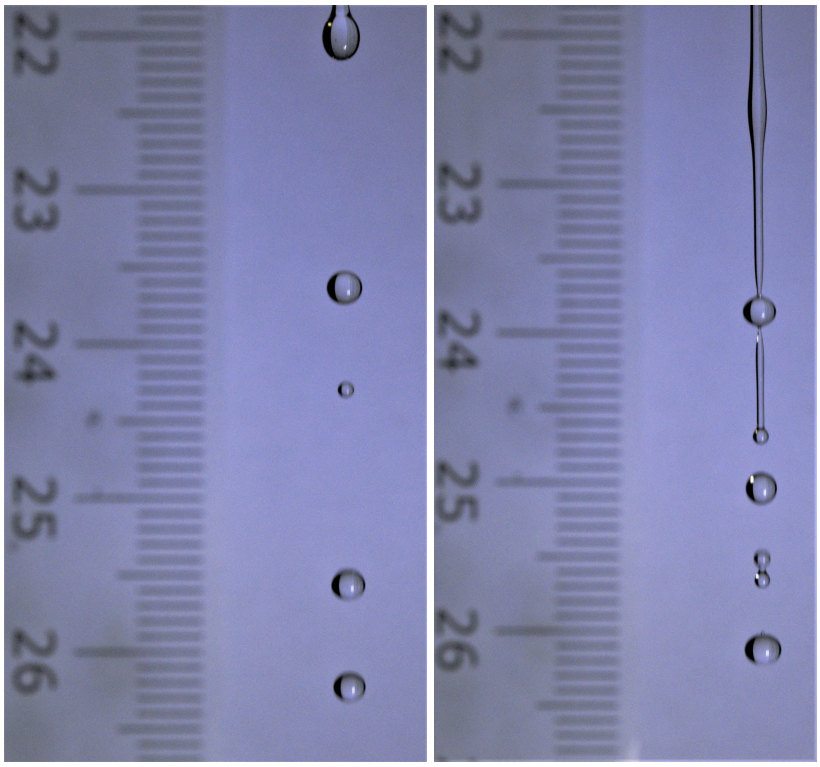


Figure 4.12: Plot of the measured breakup length $L_D$, normalized by the outer radius $2R_{out}$ versus the Ohnesorge number, signifying the effects of viscosity. The solid lines represent the measured results and the dashed lines represent the prediction by the model of equation (2.4).

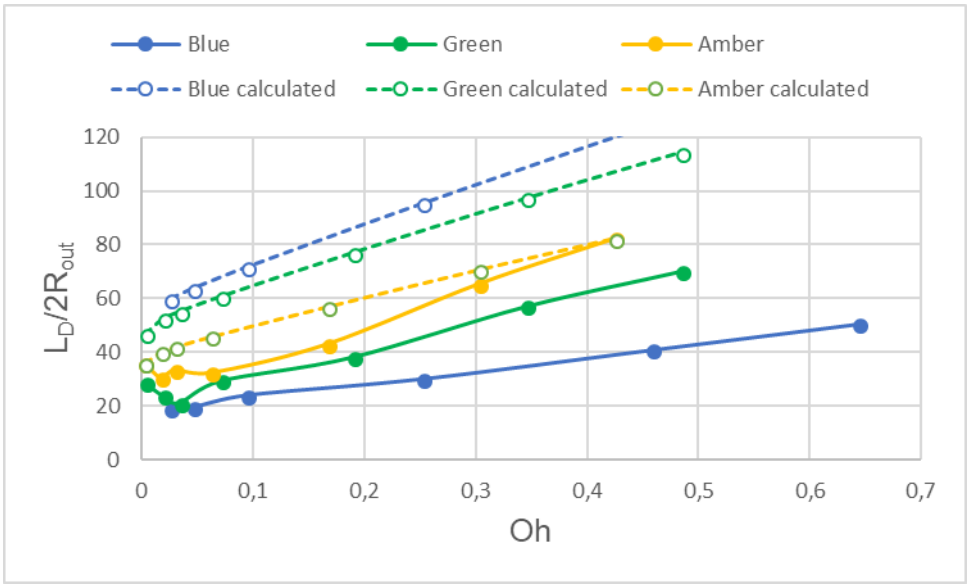

# 5

# Conclusion & Recommendations

## 5.1. Conclusion

In this work we aimed to provide a basis for further research on the topic of jet breakup. Three specific goals were set for this research: determining the effects of viscosity and nozzle diameter on the transition points from dripping to jetting mode, determining how the breakup length is affected by changes in viscosity and flow-rate, and comparing these results to predictions and presenting them in a dimensionless form.

The transition points were found for a range of nozzle diameters, and its dependencies were confirmed. Larger nozzles require larger flow-rates to reach jetting mode, while the Weber number corresponding to the nozzle-flow-rate combination decreases with increasing diameter. Meanwhile, increasing viscosity of the fluid decreased the required flow-rate (and thus Weber number) to reach jetting mode.

Qualitatively, it was found that satellite droplets formed more easily and more often in highly viscous fuids, than in relatively non-viscous fluids.

The typical length before breakup occurs was determined for most nozzles: some nozzles proved so small that the pressures became too extreme for the set-up, and were therefore left out. As expected, an increase in flow-rate led to an increase in breakup length. Similarly, increasing viscosities also led to increasing breakup lengths.

All data was eventually presented in dimensionless form, either by expressing quantities as their related dimensionless numbers or by normalizing them according to normalization standards used in literature.

Fitting the data to existing predictions proved to be difficult. For the critical Weber number corresponding to the transition, versus the Ohnesorge number for changing viscosities, no relation or trend was found.

The results of the experiments on breakup length and the critical weber number for the transition point of pure water are mismatched with the predictions intially, but grow closer and closer together with increasing nozzle diameter. It is highly likely, that the relatively small diameter of the chosen nozzles causes other variables than those researched to become significantly present in the jet breakup, thus causing divergence from the existing predictions. This would explain the increasing accuracy of the predictions with increasing nozzle diameter.

## 5.2. Recommendations

As stated in the conclusion, the relatively small diameter of the nozzles chosen for this research are suspected of having caused the mismatch between results and predictions. This suspicion might be confirmed by repeating these experiments for a large range of nozzle diameters.

Subsequently, if the previous suspicion is confirmed, further research is needed to investigate what other factors affect the jet-breakup in such a way, that their presence is only significantly present for low nozzle diameters. Similarly, if the suspicion is rejected, another explanation needs to be found for the results obtained in this report.

The effects of viscosity on the transition point showed no real trend. Research can be done to investigate whether a relation can be found between the two.

Lastly, internal velocity profiles were neglected for this report, yet it is suspected they affect the jet breakup significantly. Therefore, the effects of different velocity profiles within the nozzle could be researched.

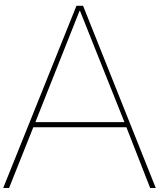

# Data tables of experiment 3

They are too large to fit on this page, they begin on the next page.

Table A.1: Raw data of experiment three, for flow-rate changes. $Q$ is the flow-rate in ml min$^{-1}$, L1-L6 are the individual measurements of the **position** where jet breakup occured for a single photograph in centimetres and La is the average breakup length in millimetres. Note that the position of the nozzle-exit has been subtracted in the formula that calculates the average: La. Position of the amber nozzle (which was longer): 16.03 cm. Position of the other nozzles: 13.83 cm.

| Nozzle | Q | L1 | L2 | L3 | L4 | L5 | L6 | La |
|---|---|---|---|---|---|---|---|---|
| | 3.00 | 14.28 | 14.15 | 14.08 | 14.2 | | | 3.475 |
| | 3.75 | 15 | 14.98 | 15 | 15.03 | | | 11.725 |
| Clear | 4.50 | 15.22 | 15.28 | 15.25 | 15.3 | | | 14.325 |
| | 5.25 | 15.52 | 15.48 | 15.65 | 15.7 | | | 17.575 |
| | 6.00 | 15.8 | 15.82 | 15.98 | 15.88 | 15.85 | 15.9 | 20.41666667 |
| | 3.20 | 14.18 | 14.08 | 14.1 | 14.21 | 14.15 | 14.1 | 3.066666667 |
| | 4.00 | 14.25 | 14.18 | 14.48 | 14.23 | | | 4.55 |
| Red | 4.80 | 15.29 | 15.28 | 15.18 | 15.2 | | | 14.075 |
| | 5.60 | 15.62 | 15.68 | 15.52 | 15.5 | | | 17.5 |
| | 6.40 | 15.8 | 15.75 | 15.92 | 15.75 | | | 19.75 |
| | 7.70 | 14.25 | 14.37 | 14.65 | 14.41 | 14.32 | | 5.7 |
| | 9.63 | 16.08 | 16.08 | 16.17 | 16.2 | | | 23.025 |
| Blue | 11.60 | 16.8 | 16.65 | 16.95 | 16.88 | 17.05 | 16.77 | 30.2 |
| | 13.50 | 17.35 | 17.35 | 17.65 | 17.4 | 17.55 | 17.45 | 36.28333333 |
| | 15.40 | 17.95 | 18.05 | 18.08 | 17.8 | | | 41.4 |
| | 22.00 | 17.33 | 17.28 | 17.44 | 17.61 | 17.62 | 17.68 | 36.63333333 |
| | 27.50 | 19.05 | 19.4 | 18.91 | 19.3 | 19 | 19.25 | 53.21666667 |
| Green | 33.00 | 20.11 | 20.35 | 20.5 | 20.45 | | | 65.225 |
| | 38.50 | 21.45 | 20.82 | 21.38 | 21.2 | | | 73.825 |
| | 44.00 | 22.5 | 22.35 | 23.5 | 23.28 | 23.15 | | 91.26 |
| | 37.00 | 22.12 | 22.16 | 21.45 | 22.02 | | | 59.075 |
| | 46.30 | 23.83 | 23.5 | 23.52 | 23.65 | | | 75.95 |
| Amber | 55.50 | 25.48 | 25.5 | 25.38 | 24.85 | | | 92.725 |
| | 64.80 | 26 | 27.3 | 26.41 | 26.4 | | | 104.975 |
| | 74.00 | 26.78 | 27.12 | 27.22 | 26.25 | 26.56 | 26.21 | 106.6 |

Table A.2: Raw data of experiment three, for viscosity changes. $\eta$ is the viscosity in mPa s, L1-L6 are the individual measurements of the **position** where jet breakup occured for a single photograph in centimetres and La is the average breakup length in millimetres. Note that the position of the nozzle-exit has been subtracted in the formula that calculates the average: La. Position of the amber nozzle (which was longer): 16.00 cm. Position of the other nozzles: 13.85 cm.

| Nozzle | glycerol wt% | $\eta$ [mPa s] | L1 [cm] | L2 [cm] | L3 [cm] | L4 [cm] | L5 [cm] | L6 [cm] | La [mm] |
|---|---|---|---|---|---|---|---|---|---|
| Blue | 0 | 1.002 | 15.22 | 15.11 | 15.27 | 15.21 | 15.33 | 15.3 | 13.9 |
| | 50 | 6 | 15.41 | 15.22 | 15.25 | 15.26 | 15.3 | 15.1 | 14.06666667 |
| | 60 | 10.8 | 15.68 | 15.29 | 15.5 | 15.75 | 15.48 | 15.79 | 17.31666667 |
| | 70 | 22.5 | 16.13 | 16.25 | 15.76 | 15.82 | 16.18 | 15.97 | 21.68333333 |
| | 80 | 60.1 | 16.72 | 16.04 | 16.81 | 17.21 | 16.8 | 17.21 | 29.48333333 |
| | 85 | 109 | 16.82 | 17.86 | 17.95 | 17.75 | 17.78 | 16.81 | 36.45 |
| | 87 | 153 | 17.33 | 17.28 | 17.44 | 17.61 | 17.62 | 17.68 | 36.43333333 |
| | | | 16.79 | 16.8 | 16.88 | 17.05 | 16.93 | 16.94 | 30.48333333 |
| Green | 0 | 1.002 | 16.78 | 16.15 | 16.29 | 16.68 | 16.53 | 16.89 | 27.03333333 |
| | 50 | 6 | 17.33 | 17.99 | 17.95 | 17.7 | 16.93 | 17.62 | 37.36666667 |
| | 60 | 10.8 | 18.8 | 18.9 | 18.42 | 18.73 | 18.91 | 18.5 | 48.6 |
| | 70 | 22.5 | 21.39 | 19.48 | 22.51 | 20.44 | 21.32 | 21.47 | 72.51666667 |
| | 80 | 60.1 | 23.62 | 22.19 | 22.89 | 22.5 | 22.55 | 22.84 | 89.15 |
| | 85 | 109 | 22.12 | 22.16 | 21.45 | 22.02 | 59.375 | 19.48 | 22.51 |
| | 87 | 153 | 20.85 | 20.13 | 21.7 | 21.51 | 20.66 | 21.65 | 50.83333333 |
| | | | 21.86 | 20.51 | 22.32 | 21.22 | 21.16 | 22.05 | 55.2 |
| Amber | 0 | 1.002 | 19.76 | 21.33 | 21.72 | 21.5 | 22 | 21.84 | 53.58333333 |
| | 50 | 6 | 23.29 | 22.19 | 24.78 | 22.19 | 24.15 | 22.08 | 71.13333333 |
| | 60 | 10.8 | 25.57 | 25.48 | 26.49 | 27.92 | 27.79 | 27.7 | 108.25 |
| | 70 | 22.5 | 19.76 | 21.33 | 21.72 | 21.5 | 22 | 21.84 | 53.58333333 |
| | 80 | 60.1 | 23.29 | 22.19 | 24.78 | 22.19 | 24.15 | 22.08 | 71.13333333 |
| | 85 | 109 | 25.57 | 25.48 | 26.49 | 27.92 | 27.79 | 27.7 | 108.25 |
| | 87 | 153 | 29.88 | 29.5 | 29.02 | 30.17 | 29.32 | 29.81 | 136.1666667 |

# B

# Backgrounds

The backgrounds on the following pages were used in the experiments. As transparent liquids (water/glycerol) act as a lens, the black outer ring/columns of the backgrounds create a black ring at the edge of the drops/jets, while they are hovering in front of the white parts. The contrast allows them to be photographed more easily.

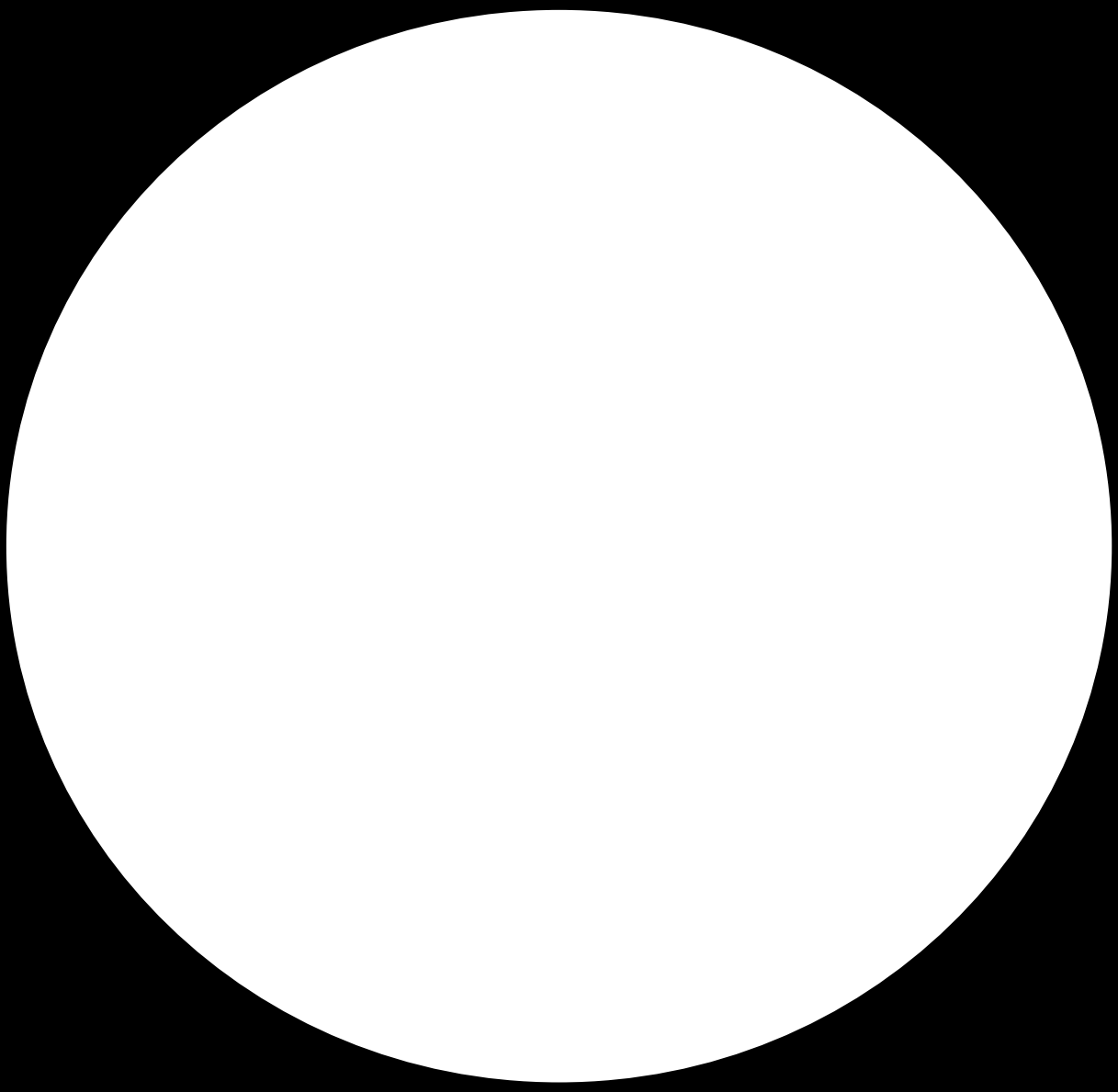

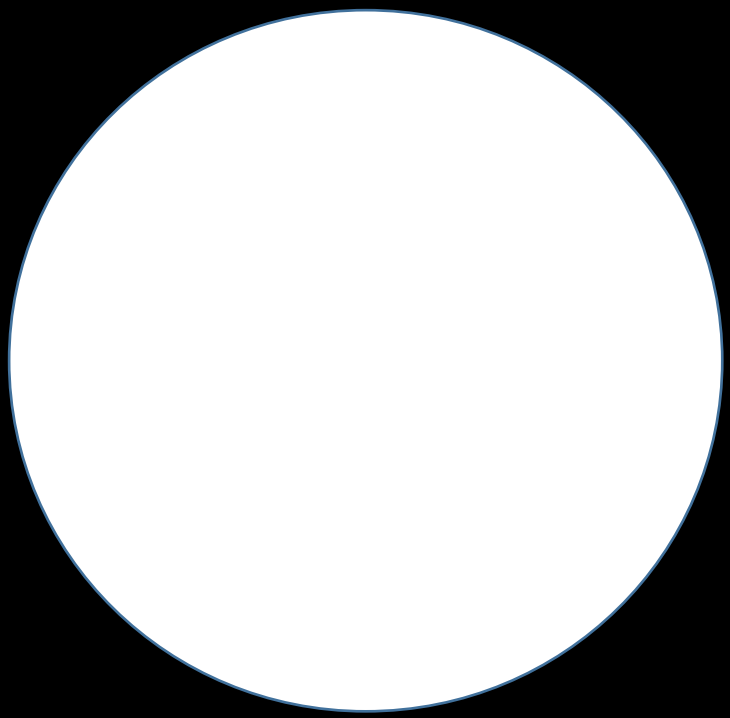

# Bibliography


[1] Harvard Apparatus. *PHD2000 Syringe Pump Series User's Manual*. Harvard Apparatus.

[2] Glycerine Producers' Association. *Physical Properties of Glycerine and its Solutions*. Glycerine Producers' Association, 1963.

[3] Oren Breslouer. Rayleigh-plateau instability: Falling jet. Master's thesis, Princeton University, 2010.

[4] T. L. Brown, H. E. jr. LeMay, B. E. Bursten, C. J. Murphy, and P. M. Woodward. *Chemistry, the Central Science*. Pearson Prentice Hall, 12th edition edition, 2012. ISBN: 978-0-321-74983-3.

[5] J. R. Castrejón-Pita, A. A. Castrejón-Pita, S. S. Thete, K. Sambath, I. M. Hutchings, J. Hinch, J. R. Lister, and O. A. Basaran. Plethora of transitions during breakup of liquid filaments. *National Academy of Sciences*, 112:4582–4587, 2015. doi: 10.1073/pnas.1418541112.

[6] Y. J. Chen and P. H. Steen. Dynamics of inviscid capillary breakup: collapse and pinchoff of a film bridge. *Journal of Fluid Mechanics*, 341:245–267, 1997.

[7] C. Clanet and J. C. Lasheras. transition from dripping to jetting. *Journal of Fluid Mechanics*, 383: 307–326, 1999. doi: 10.1017/S002211209800406.

[8] Nordson Corporation. General purpose tips, 2018. URL `http://www.nordson.com/en/divisions/efd/products/dispense-tips/general-purpose-tips`. Accessed: May 22nd, 2018.

[9] R. F. Day, J. Hinch, and J. R. Lister. Self-similar capillary pinchoff of an inviscid fluid. *Physical Review Letters*, 80:704–707, 1998.

[10] Becton Dickinson. General use syringes, catalog, 2016. URL `http://catalog.bd.com/nexus-ecat/getProductDetail?productId=309654&parentCategory=1074&parentCategoryName=Syringes&categoryId=1076&categoryName=General%20Use%20Syringes&searchUrl=`. Accessed: July, 10th, 2018.

[11] J. Eggers and E. Villermaux. Physics of liquid jets. *Report on Progress in Physics*, 71, 2008. doi: 10.1088/0034-4885/71/3/036601.

[12] H. B. Eral, E. R. Safai, B. Keshavarz, J. J. Kim, J. Lee, and P. S. Doyle. Governing principles of alginate microparticle synthesis with centrifugal forces. *Langmuir*, 32:7198–7209, 2016. doi: 10.1021/acs.langmuir.6b00806.

[13] J. B. Keller and M. J. Miksis. Surface tension driven flows. *SIAM Journal on Applied Mathematics*, 43:268–277, 1983.

[14] P. K. Kundu and I. A. Cohen. *Fluid Mechanics*. Elsevier, 4th edition edition, 2008. ISBN: 978-0-12-373735-9.

[15] S.P. Lin and R.D. Reitz. Drop and spray formation from a liquid jet. *Annual Review of Fluid Mechanics*, 30:85–105, 1998.

[16] Stanley Middleman. Stability of a viscoelastic jet. *Chemical Engineering Science*, 20:1037–1040, 1965. doi: 10.1016/0009-2509(65)80105-1.

[17] D. T. Papageorgiou. On the breakup of viscous liquid threads. *Physics of Fluids*, 7:1529–1544, 1995. doi: 10.1063/1.868540.

[18] R. D. Reitz and F. v. Bracco. *Encyclopedia of Fluid Mechanics*. Gulf publishing company, P.O. Box 2608, Houston, Texas, 77001, 1986. Chapter 10.

[19] J. B. Segur and H. E. Oberstar. Viscosity of glycerol and its aqueous solutions. *Industrial and Engineering Chemistry*, 43:2117–2120, 1951. doi: 10.1063/1.868577.

[20] M. M. C. G. Warmoeskerken and L. P. B. M. Janssen. *Transport Phenomena Data Companion*. VSSD, Leeghwaterstraat 42, 2628CA Delft, 3rd edition edition, 2006. ISBN: 90-71301-59-1.

[21] Wikipedia. Surface tension wavy jet, 2018. URL https://en.wikipedia.org/wiki/Plateau%E2%80%93Rayleigh_instability#/media/File:SurfTensWavyJet.svg. Accessed: May 4th, 2018.

[22] X. Zhang and O.A. Basaran. An experimental study of dynamics of drop formation. *Physics of Fluids*, 7:1184–1203, 1995. doi: 10.1063/1.868577.